SIAM J. NUMER. ANAL.
Vol. 54, No. 2, pp. 942–968

STABLE CELL-CENTERED FINITE VOLUME DISCRETIZATION FOR BIOT EQUATIONS*

JAN MARTIN NORDBOTTEN†

Abstract. In this paper we discuss a new discretization for the Biot equations. The discretization treats the coupled system of deformation and flow directly, as opposed to combining discretizations for the two separate subproblems. The coupled discretization has the following key properties, the combination of which is novel: (1) The variables for the pressure and displacement are co-located and are as sparse as possible (e.g., one displacement vector and one scalar pressure per cell center). (2) With locally computable restrictions on grid types, the discretization is stable with respect to the limits of incompressible fluid and small time-steps. (3) No artificial stabilization term has been introduced. Furthermore, due to the finite volume structure embedded in the discretization, explicit local expressions for both momentum-balancing forces and mass-conservative fluid fluxes are available. We prove stability of the proposed method with respect to all relevant limits. Together with consistency, this proves convergence of the method. Finally, we give numerical examples verifying both the analysis and the convergence of the method.

Key words. porous media, numerical methods, convergence

AMS subject classifications. 65M08, 65M12, 65Z05

DOI. 10.1137/15M1014280

1. Introduction.

Deformable porous media are becoming increasingly important in applications. In particular, the emergence of strongly engineered geological systems such as CO_2 storage [31, 33], geothermal energy [35], and shale-gas extraction all require analysis of the coupling of fluid flow and deformation. Beyond the subsurface, physiological processes are increasingly simulated, exploiting the Biot models [8].

With this motivation, we consider the following model problem poroelastic media [9]:

$$\nabla \cdot \boldsymbol{\pi} = \boldsymbol{f}_{\boldsymbol{u}} \quad \text{in } \Omega, \tag{1a}$$
$$\boldsymbol{\pi} = \mathbb{C} : \nabla \boldsymbol{u} - \alpha p \boldsymbol{I} \quad \text{in } \Omega, \tag{1b}$$
$$\alpha \nabla \cdot \boldsymbol{u} + \rho p + \tau \nabla \cdot \boldsymbol{q} = f_p \quad \text{in } \Omega, \tag{1c}$$
$$\boldsymbol{q} = -\boldsymbol{k} \nabla p \quad \text{in } \Omega, \tag{1d}$$
$$\boldsymbol{u} = \boldsymbol{g}_{\boldsymbol{u},D} \quad \text{on } \Gamma_{\boldsymbol{u},D}, \tag{1e}$$
$$\boldsymbol{\pi} \cdot \boldsymbol{n} = \boldsymbol{g}_{\boldsymbol{u},N} \quad \text{on } \Gamma_{\boldsymbol{u},N}, \tag{1f}$$
$$p = g_{p,D} \quad \text{on } \Gamma_{p,D}, \tag{1g}$$
$$\boldsymbol{q} \cdot \boldsymbol{n} = g_{p,N} \quad \text{on } \Gamma_{p,N}. \tag{1h}$$

Equations (1) arise from an implicit (backward Euler) time discretization of the linear Biot equations, and in this context τ represents the time-step. The domain Ω is a bounded connected polygonal subset of $\mathbb{R}^d$, with boundary $\partial\Omega = \Gamma_D \cup \Gamma_N$. The notation adopted in equations (1) utilizes the variables vector displacement ($\boldsymbol{u}$),

---

*Received by the editors March 27, 2015; accepted for publication (in revised form) February 9, 2016; published electronically March 29, 2016.

http://www.siam.org/journals/sinum/54-2/M101428.html

†Department of Mathematics, University of Bergen, N-5020 Bergen, Norway, and Department of Civil and Environmental Engineering, Princeton University, Princeton, NJ 08544 (jan.nordbotten@math.uib.no).

scalar pressure (p), tensor Biot stress ($\boldsymbol{\pi}$), and vector Darcy flux ($\boldsymbol{q}$). The spatially dependent material stiffness tensor is denoted by $\mathbb{C}$, the Biot coupling coefficient (α), the fluid compressibility (ρ), and the permeability ($\boldsymbol{k}$). We denote source-terms by f and boundary conditions as g.

All parameters are in general positive (definite) functions of space, and the discretization formulated herein considers arbitrary spatial variability of the parameter functions. Nevertheless, we will for the sake of simplicity and conciseness of presentation suppress this spatial dependence in the current section and in the convergence analysis given in section 5. Thus when parameters are treated as constants, it should be understood in the sense of, e.g., $\rho = \inf_{\boldsymbol{x}\in\Omega} \rho(\boldsymbol{x})$. For boundary conditions, we assume that both $\Gamma_{\boldsymbol{u},D}$ and $\Gamma_{u,D}$ have positive measure: The case of $\Gamma_{\boldsymbol{u},N} = \partial\Omega$ or $\Gamma_{p,N} = \partial\Omega$ can be accommodated, but the additional complications will not be of sufficient interest to merit the additional notation and loss of clarity in the presentation. Without loss of generality, we will by subtracting any smooth function satisfying the boundary conditions and correspondingly modifying the right-hand side assign all boundary conditions as homogeneous.

Under the stated conditions on parameters and boundary conditions, for reasonable forcing functions, equations (1) have a unique weak solution $(\boldsymbol{u}, p) \in (H^1(\Omega))^d \times H^1(\Omega)$ (throughout the paper, we will implicitly consider the restriction of the function spaces such that the Dirichlet boundary conditions are satisfied). Furthermore, in the case where $\tau = 0$, or, equivalently, if the medium is impermeable ($\boldsymbol{k} = 0$), the compressible Stokes equations are recovered. This implies that the regularity of the pressure is reduced, and we have a unique weak solution $(\boldsymbol{u}, p) \in (H^1(\Omega))^d \times L^2(\Omega)$. Finally, if the incompressible case is considered, $\rho = 0$, the pressure in the Stokes equations is only defined up to a constant. This motivates the following definition.

DEFINITION 1. *We denote a discretization of equations* (1) *as* robust *if there exists an estimate of the form*

$$\|\boldsymbol{u}\|_1 + \tau\|p\|_1 + \rho\|p\|_0 + |p|_0 \leq C(\|\boldsymbol{f_u}\| + \|f_g\|),$$

where the constant C is bounded independent of the small parameters ρ and τ, and we denote $|p|_0 = \inf_{p_0}\|p - p_0\|_0$.

Our interest will be in obtaining a simple discretization which is robust, which retains an explicit conservation principle for both momentum balance (1a) and mass balance (1c) and which has a co-located cell-centered data structure for both pressure and deformation. As our primary interest lies in geological porous media, we will furthermore make no assumption on the smoothness of the data beyond bounded measure.

The main difficulty associated with obtaining a robust discretization of equations (1) arises from the three saddle-point systems embodied in the formulation. In the absence of fluid pressure, (1a) and (1b) represent a saddle-point system for the solid subproblem, and, similarly, in the absence of solid deformation, (1c) and (1d) represent a saddle-point system for the fluid subproblem. Finally, if mechanical stress and fluid fluxes are eliminated, the displacement-pressure system itself is a saddle-point system.

Disregarding conservation properties, low-order standard finite elements are nevertheless not stable for the limit of incompressible solids [25, 11]. Due to the saddle-point nature of the displacement-pressure system, the displacement and pressure spaces must furthermore be chosen as a Stokes-stable pair in order to satisfy a Ladyzhenskaya–Babuska–Brezzi (LBB, or inf-sup) condition as $\rho, \tau \to 0$ [11]. For these reasons, stabilized formulations have been considered to allow for arbitrary choices of finite element spaces [8]. While their stabilization can be motivated through various formalisms, consistency is often lost. Similar problems appear for co-located finite difference discretizations. While less literature is available, a Brezzi–Pitkaranta-type [12] stabilization term has also been analyzed in the context of finite difference methods for the Biot equations [16].

A natural option in order to obtain stable discretizations while retaining the explicit conservation structure is to construct a multifield set of inf-sup stable mixed finite element spaces. The fluid subproblem can be successfully discretized by mixed finite elements [11], and much supporting literature exists for this problem. In contrast, the solid subproblem does not lend itself trivially to mixed finite elements, and although much recent literature relates to this problem, simple low-order element combinations appear to be impossible to devise [6]. A thorough numerical investigation of various combinations of mixed methods for the full Biot equations has been reported [18]. An alternative to mixed finite elements (but similar in spirit) is to use staggered grids for the mechanics and flow equations [37, 17]. The use of staggered grids resolves stability issues, but it leads to more restrictions on admissible grids and increases the technical difficulties associated with constructing efficient solvers.

A novel cell-centered finite volume (FV) method for solid displacement has recently been introduced as the multipoint stress approximation (MPSA) method by the author, for the purpose of consistent treatment of the fluid and displacement equations [27]. This class of FV methods, along with its counterpart for fluid flow, the multipoint flux approximation (MPFA) method [1], is applicable to a wide range of grids of relevance to industrial applications. In contrast to control-volume finite element methods [20], these methods are furthermore particularly well suited for problems with large material contrasts [13], as are frequently seen in subsurface flows. The MPSA and MPFA methods have recently been combined to solve the Biot equations [28]. While that paper shows applications including fractured media with complex geometries, the resulting discretization is not robust in the limit of small time-steps τ, and no theoretical analysis is provided for the coupled scheme.

Theoretical properties for MPFA methods have long been established by exploiting links to mixed finite element methods [21, 36]. However, due to the lack of simple finite element methods for elasticity and the Biot equations, of relevance for the current work is the analysis within the hybrid FV framework [14] and the recent analysis of the MPFA [3] and MPSA methods [29].

Herein, we will expand on the FV framework as developed in [29] to establish a coupled discretization for the Biot equations directly. This approach leads us to a new discretization, which we refer to as MPFA/MPSA-FV. The discretization has the following properties: (i) The discretizations of the fluid and mechanical subproblems are identical to the decoupled FV discretizations. (ii) When local variables are eliminated by static condensation (as is typical for FV methods), the resulting system of equations is in terms of cell-centered displacement and pressure only. (iii) We show that the co-located discretization is naturally stable in the sense of Definition 1 without the addition of any artificial stabilization term or stabilization parameter. (iv) The discretization is consistent with the variational FV formulation of the Biot system.

We note at this moment that Definition 1 is not sufficient to study the property of numerical locking for a nearly incompressible mechanical subproblem. In order to analyze locking, a term needs to be introduced accounting for the divergence of displacement, $\|\nabla \cdot \boldsymbol{u}\|_0$. We choose not to include this in our analysis for four reasons: (a) Fully incompressible materials are of little interest in the setting of the Biot equations, since the coupling term is exactly the compression. (b) The mechanical discretization obtained herein is in itself locking-free on most grids [29]. (c) For the Biot equations, locking-free schemes can be achieved at no additional complexity by introducing a solid pressure in the formulation [24]. (d) The analysis becomes much more complex, both in practical terms and in the sense of notation. Indeed, to illustrate points (a) and (d) we note that for incompressible materials, the left-hand side of (1c) is zero in the limit of $(\rho, \tau) \to 0$ such that no regularity of pressure is expected in this limit. This issue can be resolved by observing that within the context of a time discretization, $f_b = O(\max(\rho, \tau, \nabla \cdot \boldsymbol{u}))$; however, this indicates some of the technical issues arising in the analysis.

We structure the rest of this paper as follows: In the next section we will recall a suitable discrete functional framework. In section 3, we will define our method within the framework of variational FV methods. In section 4, we identify the cell-centered discretizations through local static condensation. The main result is stated in section 5, where we show stability and convergence of the coupled discretization. In section 6, we provide numerical results which underscore the robustness claims in all relevant parameter regimes and provides numerical convergence rates for smooth problems. Finally, section 7 concludes the paper.

2. Discrete functional framework.

In this section we give the definition of our FV mesh and discrete variables. The setting will be identical to the discrete framework used for pure elasticity in [29]. Our mesh description and discrete framework expand on those of [3], which again generalizes [14]. As this section contains no novel material, the presentation will be as brief as possible, and the reader is referred to the references for further details.

2.1. FV mesh.

We denote an FV mesh by the triplet $\mathcal{D} = (\mathcal{T}, \mathcal{F}, \mathcal{V})$, representing the mesh tessellation, faces, and vertexes, such that the following hold:

- $\mathcal{T}$ is a nonoverlapping partition of the domain Ω. Furthermore, let m_K denote the d-dimensional measure of $K \in \mathcal{T}$.
- $\mathcal{F}$ is a set of faces of the partitioning $\mathcal{T}$. We consider only cases where elements $\sigma \in \mathcal{F}$ are subsets of $(d-1)$-dimensional hyperplanes of $\mathbb{R}^d$, and with all elements $\sigma \in \mathcal{F}$ we associate the $(d-1)$-dimensional measure m_σ. Naturally, the faces must be compatible with the mesh such that for all $K \in \mathcal{T}$ there exists a subset $\mathcal{F}_K \subset \mathcal{F}$ such that $\partial K = \bigcup_{\sigma \in \mathcal{F}_K} \sigma$.
- $\mathcal{V}$ is a set of vertexes of the partitioning $\mathcal{T}$. Thus for any d faces $\sigma_i \in \mathcal{F}$, either their intersection is empty or $\bigcap_i \sigma_i = s \in \mathcal{V}$.

Note that in the above (and throughout this paper), we abuse notation by referring to the object and the index by the same notation. For example, we will by $K \in \mathcal{T}$ allow K to denote the index, as in $\mathcal{F}_K$, but also the actual subdomain of Ω, such that the expressions ∂K and $m_K = \int_K d\boldsymbol{x}$ are meaningful.

Additionally, we state the following useful subsets of the mesh triplet, which allows us to efficiently sum over neighboring cells, faces, or vertices:

- For each cell $K \in \mathcal{T}$, in addition to the faces $\mathcal{F}_K$, we denote the vertexes of K by $\mathcal{V}_K$. We will associate with each vertex $s \in \mathcal{V}_K$ a subcell of K, identified by (K, s), with a volume m_K^s such that $\sum_{s \in \mathcal{V}_K} m_K^s = m_K$.
- For each face $\sigma \in \mathcal{F}$, we denote the neighboring cells $\mathcal{T}_\sigma$ and its vertex for $\mathcal{V}_\sigma$. Note that for all internal faces $\mathcal{T}_\sigma$ will contain exactly two elements, while it contains a single element when $\sigma \subset \partial\Omega$. We will associate with each corner $s \in \mathcal{V}_\sigma$ a subface of σ, identified by (s, σ), with an area m_σ^s such that $\sum_{s \in \mathcal{V}_\sigma} m_\sigma^s = m_\sigma$.
- For each vertex $s \in \mathcal{V}$, we denote the adjacent cells by $\mathcal{T}_s$ and the adjacent

faces by $\mathcal{F}_s$.

We associate with each element $K \in \mathcal{T}$ a unique point (cell center) $\boldsymbol{x}_K \in K$ such that K is star-shaped with respect to $\boldsymbol{x}_K$, and we denote the diameter of K by d_K. Furthermore, we denote the distance between cell centers $\boldsymbol{x}_K$ and $\boldsymbol{x}_L$ as $d_{K,L} = |\boldsymbol{x}_K - \boldsymbol{x}_L|$. The grid diameter is denoted by $h = \max_{K\in\mathcal{T}} d_K$.

We associate with each face σ its outward normal vector with respect to the cell $K \in \mathcal{T}_\sigma$ as $\boldsymbol{n}_{K,\sigma}$ and the Euclidean distance to the cell center as d_K^σ. For each subface (s,σ), we denote the subface center as $\boldsymbol{x}_\sigma^s$ and a set of quadrature points on (s,σ) as $\mathcal{G}_\sigma^s$. With each quadrature point $\beta \in \mathcal{G}_\sigma^s$ we associate the position $\boldsymbol{x}_\beta$ and weight ω_β. In general, we will choose sufficient quadrature points for exact integration of second-order polynomials; however, for simplex grids, it is advantageous to choose only a single quadrature point.

The above definition covers all two-dimensional grids of interest and quite general three-dimensional grids. However, the definition disallows three-dimensional grids with curved surfaces (e.g., distorted cubes). A more general formulation appears to be practicable [3] but would come at the expense of additional notation and analysis.

Regularity assumptions on the discretization $\mathcal{D}$ are detailed elsewhere (see, e.g., [14]); we will in the interest of simplicity of exposition henceforth assume that the classical grid regularity parameters (grid skewness, internal cell angles, and coordination number of vertexes) do not deteriorate.

2.2. Discrete variables and norms. We detail the three discrete spaces used in our analysis below. They represent, respectively, the space of cell variables $\mathcal{H}_\mathcal{T}$, cell and discontinuous face variables $\mathcal{H}_\mathcal{D}$, and cell and continuous face variables $\mathcal{H}_\mathcal{C}$.

The following discrete space is classical [14] and is the space where the final cell-centered discretization will take its values.

Definition 2. *For the mesh $\mathcal{T}$, let $\mathcal{H}_\mathcal{T}(\Omega) \subset L^2(\Omega)$ be the set of piecewise constant functions on the cells of the mesh $\mathcal{T}$.*

As with the dual interpretation of the elements $K \in \mathcal{T}$, the space $\mathcal{H}_\mathcal{T}(\Omega)$ is isomorphic to the space of discrete variables associated with the cell-centered points $\boldsymbol{x}_K$. There should also be no cause for confusion in the following when we also work with the vector-valued spaces, then denoted by bold $\boldsymbol{\mathcal{H}}_\mathcal{T}$.

For the space $\mathcal{H}_\mathcal{T}$ we introduce the inner product

$$[u,v]_\mathcal{T} = \sum_{K\in\mathcal{T}} \sum_{\sigma\in\mathcal{F}_K} \frac{m_\sigma}{d_{K,\sigma}} (\gamma_\sigma u - u_K)(\gamma_\sigma v - v_K)$$

and its induced norm

$$\|u\|_\mathcal{T} = ([u,u]_\mathcal{T})^{1/2}.$$

Here the operator $\gamma_\sigma u$ interpolates the piecewise constant values of $\mathcal{H}_\mathcal{T}$ onto the faces of the mesh, weighted by the distances $d_{K,\sigma}$:

$$\gamma_\sigma u = \left(\sum_{K\in\mathcal{T}_\sigma} \frac{u_K}{d_{K,\sigma}} \right) \Big/ \left(\sum_{K\in\mathcal{T}_\sigma} d_{K,\sigma}^{-1} \right) \quad \text{for all } \sigma \in \mathcal{F};\ \sigma \notin \Gamma_D.$$

For Dirichlet boundary edges, $\sigma \in \Gamma_D$, we take $\gamma_\sigma u = 0$. Equivalently, the operator $\gamma_\sigma u$ can be defined as the value which minimizes the definition of the norm $\|u\|_\mathcal{T}$. The norm defined above is naturally identified as an H^1-type norm for the space. We will furthermore need the discrete L^2 inner product for $\mathcal{H}_\mathcal{T}$

$$[u,v]_{\mathcal{T},0} = \sum_{K\in\mathcal{T}} m_K u_K v_K$$

and its induced norm

$$\|u\|_{\mathcal{T},0} = ([u,u]_{\mathcal{T},0})^{1/2}.$$

Definition 3. *For the mesh triplet $\mathcal{D}$, let $\mathcal{H}_\mathcal{D}$ be the set of real scalars $(u_K, u_{K,s}^{\sigma,\beta})$ for all $K \in \mathcal{T}$, for all $(s,\sigma) \in \mathcal{V}_K \times \mathcal{F}_K$, and for all $\beta \in \mathcal{G}_\sigma^s$.*

The space $\mathcal{H}_\mathcal{D}$ thus contains one unknown per cell, in addition to multiple unknowns on each interior subface. This space was introduced in order to control the space of rigid body motions when discretizing the mechanical subproblem [27]. As above, we will immediately take $u_{K,s}^{\sigma,\beta} = 0$ for all $\sigma \in \Gamma_D$.

We denote for all internal subfaces $[[u]]_s^{\sigma,\beta} = u_{R,s}^{\sigma,\beta} - u_{L,s}^{\sigma,\beta}$ for $u \in \mathcal{H}_\mathcal{D}$ and $\mathcal{T}_\sigma = \{R, L\}$ as the jump in the discrete function u across that edge. We will also need a notion of an average face value, and we denote similarly for all internal subfaces $\langle u\rangle_s^\sigma = \sum_{\beta\in\mathcal{G}_s^\sigma} \omega_\beta \frac{u_{R,s}^{\sigma,\beta}+u_{L,s}^{\sigma,\beta}}{2}$. For boundary edges $\sigma \in \partial\Omega$, only one function value is available, and we define $[[u]]_s^{\sigma,\beta} = 0$ and $\langle u\rangle_s^\sigma = \frac{1}{m_s^\sigma}\sum_{\beta\in\mathcal{G}_s^\sigma} \omega_\beta u_{R,s}^{\sigma,\beta}$. We now associate with the space $\mathcal{H}_\mathcal{D}$ the inner product

$$\begin{aligned}[u,v]_\mathcal{D} = \sum_{K\in\mathcal{T}} \sum_{s\in\mathcal{V}_K} \sum_{\sigma\in\mathcal{F}_s\cap\mathcal{F}_K} & \frac{m_K^s}{d_{K,\sigma}^2}(u_K - \langle u\rangle_s^\sigma)(v_K - \langle v\rangle_s^\sigma) \\ & + \frac{m_K^s}{d_{K,\sigma}^2}\frac{1}{m_s^\sigma}\sum_{\beta\in\mathcal{G}_s^\sigma} \omega_\beta [[u]]_s^{\sigma,\beta}[[v]]_s^{\sigma,\beta}\end{aligned}$$

and the induced norm

$$\|u\|_\mathcal{D} = [u,u]_\mathcal{D}^{1/2}.$$

Definition 4. *For the mesh triplet $\mathcal{D}$, let $\mathcal{H}_\mathcal{C}$ be the set of real scalars (u_K, u_s^σ) for all $K \in \mathcal{T}$ and for all $(s,\sigma) \in \mathcal{V}_K \times \mathcal{F}_K$.*

This last space is essential for obtaining the FV structure of the scheme [3].

By introducing the natural interpolation operator $\Pi_\mathcal{D}\colon \mathcal{H}_\mathcal{C} \to \mathcal{H}_\mathcal{D}$ as $(\Pi_\mathcal{D} u)_K = u_K$ and $(\Pi_\mathcal{D} u)_{K,s}^{\sigma,\beta} = u_s^\sigma$ for all $K \in \mathcal{T}$ and for all $(s,\sigma) \in \mathcal{V}_K \times \mathcal{F}_K$, we can immediately define the inner product

$$[u,v]_\mathcal{C} = [\Pi_\mathcal{D} u, \Pi_\mathcal{D} v]_\mathcal{D}$$

and the induced norm

$$\|u\|_\mathcal{C} = [u,u]_\mathcal{C}^{1/2}.$$

In addition to the interpolation operator defined above, we shall need a few more operators to move between function spaces:

- Let the operator $\Pi_\mathcal{T}\colon \mathcal{H}_\mathcal{D} \to \mathcal{H}_\mathcal{T}$ be defined as $(\Pi_\mathcal{T} u)(x) = u_K$ for all $x \in K$ and $K \in \mathcal{T}$. Furthermore, as there should be no reason for confusion, we also define $\Pi_\mathcal{T}\colon \mathcal{H}_\mathcal{C} \to \mathcal{H}_\mathcal{T}$ as $(\Pi_\mathcal{T} u)(x) = (\Pi_\mathcal{T}\Pi_\mathcal{D} u)(x) = u_K$ for all $x \in K$ and $K \in \mathcal{T}$. Finally, we also write $\Pi_\mathcal{T}\colon C(\Omega) \to \mathcal{H}_\mathcal{T}$ as $(\Pi_\mathcal{T} u)(x) = u(x_K)$ for all $x \in K$ and $K \in \mathcal{T}$.
- Let the operator $\Pi_\mathcal{C}\colon \mathcal{H}_\mathcal{D} \to \mathcal{H}_\mathcal{C}$ be defined as $(\Pi_\mathcal{C} u)_K = u_K$ and $(\Pi_\mathcal{C} u)_s^\sigma = \langle u\rangle_s^\sigma$ for all $K \in \mathcal{T}$ and for all $(s,\sigma) \in \mathcal{V}_K \times \mathcal{F}_K$.

The spaces defined above satisfy the following inequalities:

- *Discrete Poincaré inequality* [14]: For all $u \in \mathcal{H}_\mathcal{T}$,

$$\|u\|_{\mathcal{T},0} \le C_P \|u\|_\mathcal{T}.$$

- *Inverse inequality* [14]: For all $u \in \mathcal{H}_\mathcal{T}$,

$$\|u\|_{\mathcal{T},0} \geq \sqrt{d}h\|u\|_\mathcal{T}.$$

- *Relationship between $\mathcal{H}_\mathcal{T}$ and $\mathcal{H}_\mathcal{C}$* [3]: For all $u \in \mathcal{H}_\mathcal{C}$,

$$\|\Pi_\mathcal{T} u\|_\mathcal{T} \leq \sqrt{d}\|u\|_\mathcal{C}.$$

- *Relationship between $\mathcal{H}_\mathcal{C}$ and $\mathcal{H}_\mathcal{D}$ (trivial from definitions)*: For all $u \in \mathcal{H}_\mathcal{D}$,

$$\|\Pi_\mathcal{C} u\|_\mathcal{C} \leq \|u\|_\mathcal{D}.$$

Finally, we introduce local spaces $\mathcal{H}_{\mathcal{D},s} \subset \mathcal{H}_\mathcal{D}$ for each $s \in \mathcal{V}$ defined such that $u \in \mathcal{H}_{\mathcal{D},s}$ if $u_{K,t}^{\sigma,\beta} = 0$ for all $t \in \mathcal{V}$ with $t \neq s$ and $u_K = 0$ if $s \notin \mathcal{V}_K$. Similarly, $\mathcal{H}_{\mathcal{T},s}$ and $\mathcal{H}_{\mathcal{C},s}$ are defined through the operators defined above. The local spaces have the natural (semi-)norms, which to be precise are given for all $u \in \mathcal{H}_\mathcal{D}$ as

$$\|u\|_{\mathcal{D},s}^2 = \sum_{K \in \mathcal{T}_s} \sum_{\sigma \in \mathcal{F}_s \cap \mathcal{F}_K} \frac{m_K^s}{d_{K,\sigma}^2}(u_K - \langle u \rangle_s^\sigma)^2 + \frac{m_K^s}{d_{K,\sigma}^2} \frac{1}{m_s^\sigma} \sum_{\beta \in \mathcal{G}_s^\sigma} \omega_\beta([[u]]_s^{\sigma,\beta})^2$$

and for all $u \in \mathcal{H}_\mathcal{T}$ as

$$\|u\|_{\mathcal{T},s}^2 = \sum_{K \in \mathcal{T}_s} \sum_{\sigma \in \mathcal{F}_s \cap \mathcal{F}_K} \frac{m_\sigma^s}{d_{K,\sigma}}(\gamma_\sigma u - u_K)^2$$

such that both

$$\|u\|_\mathcal{D}^2 = \sum_{s \in \mathcal{V}} \|u\|_{\mathcal{D},s}^2 \quad \text{and} \quad \|u\|_\mathcal{T}^2 = \sum_{s \in \mathcal{V}} \|u\|_{\mathcal{T},s}^2.$$

3. Discrete mixed variational FV discretizations for Biot.

In this section, we will utilize the spaces defined in section 2 to establish a cell-centered FV method for the Biot equations. The approach builds on the discrete mixed variational formulation of existing methods for the pressure (cf. [3, 29]) and displacement equations [29]. The key novel aspects arise due to the coupling terms arising in equations (1). The careful treatment of these terms will lead to a naturally stable discretization, which improves on the method presented in [28]. These issues will be crucial in the analysis and further highlighted in the numerical examples.

Our approach will exploit a discrete variational formalism for the Biot problem; thus we introduce the variational form of equations (1): Find $(\boldsymbol{u}, p) \in \boldsymbol{H}^1 \times H^1$ such that

$$(\mathbb{C} : \nabla \boldsymbol{u}, \nabla \boldsymbol{v}) - (\alpha p, \nabla \cdot \boldsymbol{v}) = -(\boldsymbol{f_u}, \boldsymbol{v}) \qquad \text{for all } \boldsymbol{v} \in \boldsymbol{H}^1, \tag{2a}$$

$$-(\nabla \cdot \boldsymbol{u}, \alpha r) - (\rho p, r) - \tau(k \nabla p, \nabla r) = -(f_p, r) \quad \text{for all } r \in H^1. \tag{2b}$$

While this form of the equation hides the stress and flux expressions, it will be implied throughout (and made explicit in section 3.2) that the methods considered herein allow for explicit and local extraction of mass conservative fluid fluxes, as well as momentum conserving surface tractions. It is also important to note that integration by parts is essential for the coupling term in (2a), in order for the system to still be well defined in the limit $\tau \to 0$, when regularity of p is reduced.

3.1. Method formulation. Will formulate our discretizations on a discrete variational form, based on equations (1). To obtain both an FV structure and a consistent method, we follow previous work [4, 27, 3] and introduce two notions of a discrete gradient. First, we note that the discrete divergence provides by duality a definition of a gradient, which thus exactly preserves the FV structure of the governing equations for each cell $K \in \mathcal{T}$.

DEFINITION 5. *For each $K \in \mathcal{T}$ and each $s \in \mathcal{V}_K$, we define the* FV gradient *for all $\boldsymbol{u} \in \boldsymbol{\mathcal{H}}_{\mathcal{C}}$:*

$$(\widetilde{\nabla}\boldsymbol{u})_K^s = \frac{1}{m_K^s} \sum_{\sigma \in \mathcal{F}_K \cap \mathcal{F}_s} m_\sigma^s (\langle \boldsymbol{u} \rangle_{K,s}^\sigma - \boldsymbol{u}_K) \otimes \boldsymbol{n}_{K,\sigma}. \tag{3}$$

For the definition to make sense, we need to specify the averaging notation in the natural way, that is, $\langle \boldsymbol{u} \rangle_{K,s}^\sigma = \frac{1}{m_s^\sigma} \sum_{\beta \in \mathcal{G}_s^\sigma} \omega_\beta u_{K,s}^{\sigma,\beta}$. We comment that in previous work the FV gradient has been referred to as the "convergent gradient" [3]. The FV gradient does not enjoy strong convergence properties, and thus a notion of a gradient which is exact for locally multilinear discrete functions is needed.

DEFINITION 6. *For each $K \in \mathcal{T}$ and each $s \in \mathcal{V}_K$, we define the* consistent gradient *for all $\boldsymbol{u} \in \boldsymbol{\mathcal{H}}_{\mathcal{D}}$:*

$$(\overline{\nabla}\boldsymbol{u})_K^s = \sum_{\sigma \in \mathcal{F}_K \cap \mathcal{F}_s} (\langle \boldsymbol{u} \rangle_{K,s}^\sigma - \boldsymbol{u}_K) \otimes \boldsymbol{g}_{K,\sigma}^s. \tag{4}$$

In order to satisfy the desired consistency property that $(\overline{\nabla}\boldsymbol{u})_K^s$ is exact for linear displacements, the vectors $\boldsymbol{g}_{K,\sigma}^s$ must satisfy the system of equations

$$\boldsymbol{I}_2 = (\overline{\nabla}\boldsymbol{x})_K^s = \sum_{\sigma \in \mathcal{F}_K \cap \mathcal{F}_s} (\langle \boldsymbol{x} \rangle_{K,s}^\sigma - \boldsymbol{x}_K) \otimes \boldsymbol{g}_{K,\sigma}^s. \tag{5}$$

Here $\boldsymbol{I}_2$ is the d-dimensional second-order identity tensor. The vectors $\boldsymbol{g}_{K,\sigma}^s$ are unique for the grids considered herein but may be nonunique for more general three-dimensional grids [3].

For both discrete gradients, the corresponding divergence is obtained either by taking the trace of the gradient or, equivalently, by replacing the outer product by a dot product. Note that the consistent and FV gradients are defined on the two distinct discrete spaces $\boldsymbol{\mathcal{H}}_{\mathcal{D}}$ and $\boldsymbol{\mathcal{H}}_{\mathcal{C}}$, respectively.

A consistent FV formulation is now obtained by using the FV gradient for the test functions and the consistent gradient otherwise. With this in mind, we introduce the following bilinear forms. For all $(\boldsymbol{u}, \boldsymbol{v}) \in \boldsymbol{\mathcal{H}}_{\mathcal{D}} \times \boldsymbol{\mathcal{H}}_{\mathcal{C}}$ and $(p, r) \in \mathcal{H}_{\mathcal{D}} \times \mathcal{H}_{\mathcal{C}}$,

$$a_{\mathcal{D}}(\boldsymbol{u}, \boldsymbol{v}) = \sum_{K \in \mathcal{T}} \sum_{s \in \mathcal{V}_K} m_K^s \big(\mathbb{C}_K : (\overline{\nabla}\boldsymbol{u})_K^s : (\widetilde{\nabla}\boldsymbol{v})_K^s\big), \tag{6}$$

$$c_{\mathcal{D}}(p, r) = \sum_{K \in \mathcal{T}} \sum_{s \in \mathcal{V}_K} m_K^s \big(k_K (\overline{\nabla} p)_K^s \cdot (\widetilde{\nabla} r)_K^s\big) \tag{7}$$

with the coupling terms defined for all

$$b_{\mathcal{D},1}(\boldsymbol{u}, r) = -\sum_{K \in \mathcal{T}} \alpha_K (\Pi_{\mathcal{T}} r)_K \sum_{s \in \mathcal{V}_K} m_K^s (\overline{\nabla} \cdot \boldsymbol{u})_K^s, \tag{8}$$

$$b_{\mathcal{D},2}^T(p, \boldsymbol{v}) = -\sum_{K \in \mathcal{T}} \alpha_K (\Pi_{\mathcal{T}} p)_K \sum_{s \in \mathcal{V}_K} m_K^s (\widetilde{\nabla} \cdot \boldsymbol{v})_K^s. \tag{9}$$

Note that the coupling terms are not in general transposes, due to the different discrete differential operators. Thus the transpose notation is used to indicate that the terms have a familiar structure.

To close the system, we need to associate the degrees of freedom in $\mathcal{H}_{\mathcal{D}}$ with an appropriate polynomial order and ensure a suitable degree of continuity [29]. Following the general paradigm for MPFA and MPSA methods [1, 27], we require the solution to be locally linear on each subcell associated with $(K,s) \in \mathcal{T} \times \mathcal{V}_K$ and consistent with the gradient $\overline{\overline{\nabla}}$. This is expressed through a bilinear form defined for all $((\boldsymbol{u},p),\boldsymbol{w}) \in (\boldsymbol{\mathcal{H}}_{\mathcal{D}} \times \mathcal{H}_{\mathcal{D}}) \times (\boldsymbol{\mathcal{H}}_{\mathcal{D}} \times \mathcal{H}_{\mathcal{D}})$ such that

(10)
$$d_{\mathcal{D}}((\boldsymbol{u},p),\boldsymbol{w}) = \sum_{K\in\mathcal{T}}\sum_{s\in\mathcal{V}_K}\sum_{\sigma\in\mathcal{F}_s}\sum_{\beta\in\mathcal{G}_\sigma^s}\big((\boldsymbol{u},p)_{K,s}^{\sigma,\beta} - (\boldsymbol{u},p)_K - (\overline{\overline{\nabla}}(\boldsymbol{u},p))_K^s\cdot(\boldsymbol{x}_\beta-\boldsymbol{x}_K)\big) \cdot \big(\boldsymbol{w}_{K,s}^{\sigma,\beta} - \boldsymbol{w}_K - (\overline{\overline{\nabla}}\boldsymbol{w})_K^s\cdot(\boldsymbol{x}_\beta-\boldsymbol{x}_K)\big).$$

Finally, weak continuity is enforced by minimizing jumps at quadrature points for both the pressure and the displacement, yielding the symmetric bilinear form

$$e_{\mathcal{D}}\big((\boldsymbol{u},p),\boldsymbol{w}\big) = \sum_{s\in\mathcal{V}}\sum_{\sigma\in\mathcal{F}_s}\frac{\nu_s^\sigma}{m_s^\sigma}\sum_{\beta\in\mathcal{G}_\sigma^s}\omega_\beta[[(\boldsymbol{u},p)]]_s^{\sigma,\beta}\cdot[[\boldsymbol{w}]]_s^{\sigma,\beta}. \tag{11}$$

The positive weights ν_s^σ can in principle be chosen arbitrarily; however, a weighted harmonic mean of the constitutive functions of the nearby cells $\mathcal{T}_\sigma$ seems beneficial in practice [27]. The full discrete problem is a constrained minimization problem, whose solution satisfies the following mixed variational system: Find $((\boldsymbol{u}_{\mathcal{D}},p_{\mathcal{D}}),(\boldsymbol{y}_{\mathcal{C}},y_{\mathcal{C}}),\boldsymbol{y}_{\mathcal{D}}) \in (\boldsymbol{\mathcal{H}}_{\mathcal{D}}\times\mathcal{H}_{\mathcal{D}})\times(\boldsymbol{\mathcal{H}}_{\mathcal{C}}\times\mathcal{H}_{\mathcal{C}})\times(\boldsymbol{\mathcal{H}}_{\mathcal{D}}\times\mathcal{H}_{\mathcal{D}})$ such that the physical constraints

$$a_{\mathcal{D}}(\boldsymbol{u}_{\mathcal{D}},\boldsymbol{v}) + b_{\mathcal{D},2}^T(p_{\mathcal{D}},\boldsymbol{v}) = -\int_\Omega \boldsymbol{f}_{\boldsymbol{u}}\cdot\Pi_{\mathcal{T}}\boldsymbol{v}\,d\boldsymbol{x} \quad \text{for all } \boldsymbol{v}\in\boldsymbol{\mathcal{H}}_{\mathcal{C}}, \tag{12}$$

$$b_{\mathcal{D},1}(\boldsymbol{u}_{\mathcal{D}},r) - [\rho_{\mathcal{T}}\Pi_{\mathcal{T}}p_{\mathcal{D}},\Pi_{\mathcal{T}}r]_{\mathcal{T},0} - \tau c_{\mathcal{D}}(p_{\mathcal{D}},r) = -\int_\Omega f_p\cdot\Pi_{\mathcal{T}}r\,d\boldsymbol{x} \quad \text{for all } r\in\mathcal{H}_{\mathcal{C}} \tag{13}$$

and the piecewise linear approximation

$$d_{\mathcal{D}}\big((\boldsymbol{u}_{\mathcal{D}},p_{\mathcal{D}}),\boldsymbol{w}\big) = 0 \quad \text{for all } \boldsymbol{w}\in(\boldsymbol{\mathcal{H}}_{\mathcal{D}}\times\mathcal{H}_{\mathcal{D}}) \tag{14}$$

hold subject to the solution constrained minimization

(15)
$$e_{\mathcal{D}}\big((\boldsymbol{u}_{\mathcal{D}},p_{\mathcal{D}}),(\boldsymbol{w},w)\big) + a_{\mathcal{D}}(\boldsymbol{w},\boldsymbol{y}_{\mathcal{C}}) + b_{\mathcal{D},1}(\boldsymbol{w},y_{\mathcal{C}}) + b_{\mathcal{D},2}^T(w,\boldsymbol{y}_{\mathcal{C}}) - [\rho_{\mathcal{T}}\Pi_{\mathcal{T}}w_{\mathcal{D}},\Pi_{\mathcal{T}}y_{\mathcal{C}}]_{\mathcal{T},0} - \tau c(w,y_{\mathcal{C}}) + d_{\mathcal{D}}\big((\boldsymbol{w},w),\boldsymbol{y}_{\mathcal{D}}\big) = 0 \quad \text{for all } (\boldsymbol{w},w)\in(\boldsymbol{\mathcal{H}}_{\mathcal{D}}\times\mathcal{H}_{\mathcal{D}}).$$

In (13) and (15), we have introduced the shorthand $\rho_{\mathcal{T}} = \Pi_{\mathcal{T}}\rho$. The components $\boldsymbol{y}_{\mathcal{C}}$ and $\boldsymbol{y}_{\mathcal{D}}$ are simply Lagrange multipliers for the constrained minimization problem and will not be of further interest. After local static condensation (as made explicit below), they will not appear in the final cell-centered method.

Equations (12)–(15) allow us to define the discrete mixed variational formulation considered herein.

Definition 7. *We refer to* (12)–(15) *as the* discrete mixed variational FV formulation for the Biot equations.

Comment 8. *Throughout this paper we will discuss the general setting where* $\overline{\nabla} \neq \widetilde{\nabla}$. *However, it is well known that in the special case of simplex grids a symmetric method can be obtained by using a single quadrature point (see, e.g.,* [13, 3, 27]*). All the results for the general setting applies to this case, with some simplifications which will be noted when relevant.*

3.2. FV structure. In the absence of the coupling terms (e.g., with $\alpha = 0$ in the bilinear form $b_{\mathcal{D}}$), the discrete mixed variational FV formulation as given in (12)–(15) is identical to the discretizations for elasticity and flow analyzed previously [29]. Furthermore, if the set of Gauss quadrature points $\mathcal{G}_s^\sigma$ is reduced to a single point per subinterface (s, σ), the discretization for the flow problem reduces to the well-known MPFA-FV scheme [3, 1].

The FV structure arises due to the definition of the FV gradients $\widetilde{\nabla}$. Indeed, we see that (with reference to a canonical basis for $\mathcal{H}_{\mathcal{C}}$) the degrees of freedom associated with cell centers imply that, e.g., (13) can be equivalently rewritten as

$$\tau \sum_{\sigma \in \mathcal{F}_K} m_\sigma q_K^\sigma(p_{\mathcal{D}}) = \int_K f_p \, d\boldsymbol{x} - \sum_{s \in \mathcal{V}_K} [m_K^s \alpha_K (\overline{\nabla} \cdot \boldsymbol{u})_K^s - \rho_K m_K p_K] \quad \text{for all } K \in \mathcal{T}, \tag{16}$$

where the normal fluxes q_K^σ are defined as

$$q_K^\sigma(p_{\mathcal{D}}) = -\left[\frac{1}{m_\sigma} \sum_{s \in \mathcal{V}_K} m_\sigma^s \boldsymbol{k}_K (\overline{\nabla} p)_K^s\right] \cdot \boldsymbol{n}_{K,\sigma}. \tag{17}$$

Furthermore, the degrees of freedom associated with subface variables in $\mathcal{H}_{\mathcal{C}}$ imply that, for all internal faces σ, equation (13) reduces to (for $\{K, L\} = \mathcal{T}_\sigma$)

$$q_K^\sigma(p_{\mathcal{D}}) = -q_L^\sigma(p_{\mathcal{D}}). \tag{18}$$

Equations (16) and (18) represent the conservation structure of the scheme, while (17) provides an explicit local expression for the fluid normal flux. Together these features identify the scheme as an FV method.

The FV structure arises in the same sense for the mechanical subproblem. First, we introduce the notion of traction $\boldsymbol{T}(\boldsymbol{n})$, which is the force on an internal surface with normal vector $\boldsymbol{n}$ and is related to the stress as $\boldsymbol{T}(\boldsymbol{n}) = \boldsymbol{\pi} \cdot \boldsymbol{n}$. In the continuous setting, it is the balance of tractions which leads to equations (1) [34]. Now we note that (12) can be rewritten (with $\boldsymbol{v} \in \boldsymbol{\mathcal{H}}_{\mathcal{T}}$) as

$$\sum_{\sigma \in \mathcal{F}_K} m_\sigma \boldsymbol{T}_K^\sigma(\boldsymbol{u}_{\mathcal{D}}, p_{\mathcal{D}}; \boldsymbol{n}_{K,\sigma}) = \int_K \boldsymbol{f}_{\boldsymbol{u}} \, d\boldsymbol{x} \quad \text{for all } K \in \mathcal{T}. \tag{19}$$

Here again we note the explicit definition of the traction $\boldsymbol{T}_K^\sigma$ as

$$\boldsymbol{T}_K^\sigma(\boldsymbol{u}_{\mathcal{D}}, p_{\mathcal{D}}; \boldsymbol{n}_{K,\sigma}) = \left[\frac{1}{m_\sigma} \sum_{s \in \mathcal{V}_K} m_\sigma^s \big(\mathbb{C}_K : (\overline{\nabla} \boldsymbol{u})_K^s - \alpha_K p_K \boldsymbol{I}_2\big)\right] \cdot \boldsymbol{n}_{K,\sigma}. \tag{20}$$

And finally, also the continuity of tractions reduces to (again for $\{K, L\} = \mathcal{T}_\sigma$)

$$\boldsymbol{T}_K^\sigma(\boldsymbol{u}_{\mathcal{D}}, p_{\mathcal{D}}; \boldsymbol{n}_{K,\sigma}) = -\boldsymbol{T}_L^\sigma(\boldsymbol{u}_{\mathcal{D}}, p_{\mathcal{D}}; \boldsymbol{n}_{L,\sigma}). \tag{21}$$

It is important to note that both the momentum balance (see (19)) and the continuity (see (21)) are written directly in terms of tractions derived from the Biot stress. This guarantees the correct notion of force balance in the method, and it will be reflected in the structure of the methods, as seen in the subsequent sections. Furthermore, the fact that the normal flux depends only on pressure in (17), while the tractions depend on both displacement and pressure in (20), is consistent with the governing physics of equations (1), and it presages the discrete structure which is revealed in (28).

The FV structure revealed by (16)–(21) motivates the nomenclature of Definition 7.

4. Local problems and cell-centered discretization.

To obtain a method of practical applicability, and in particular a cell-centered scheme, it is necessary to be able to perform a local static condensation within the framework of (12)–(15). For mixed finite element formulations, this is frequently achieved by numerical quadrature (see, e.g., [32, 38, 21]); however, in our setting no further approximations are required. Indeed, we will see that (12)–(15) by construction allow for local static condensation to be performed. Such constructions are classical for FV methods for elliptic problems (see, e.g., [14, 2]).

As noted, the discrete mixed variational problem (12)–(15) is a direct generalization of the discretizations for elasticity and fluid pressure analyzed in [29]. Importantly, this implies that the local problems, and hence many components of the coupled discretization, are identical to their decoupled counterparts. This will greatly simplify the subsequent analysis.

The structure of this section is as follows. We will first clearly identify the local problems and show that the static condensation required to reach a cell-centered formulation is well-posed. This also induces an interpolation from the space $\boldsymbol{\mathcal{H}}_\mathcal{T} \times \mathcal{H}_\mathcal{T}$ into $\boldsymbol{\mathcal{H}}_\mathcal{D} \times \mathcal{H}_\mathcal{D}$. This interpolation forms the key to analyzing the method and allows us to express the cell-centered discretization.

4.1. Local problems.

The variational multiscale (VMS) methods [19] as applied to mixed problems [5, 26] provides a suitable framework for formalizing the localization and static condensation of the system problem (12)–(15). We note that this use of the VMS framework is different from the approach taken when deriving additional stabilization terms [8]. By identifying the cell-centered values $(\boldsymbol{\mathcal{H}}_\mathcal{T} \times \mathcal{H}_\mathcal{T})$ as the space of coarse variables, and taking face values, denoted by $(\boldsymbol{\mathcal{H}}_\mathcal{F} \times \mathcal{H}_\mathcal{F}) = (\boldsymbol{\mathcal{H}}_\mathcal{D} \times \mathcal{H}_\mathcal{D}) \setminus (\boldsymbol{\mathcal{H}}_\mathcal{T} \times \mathcal{H}_\mathcal{T})$, as the space of fine variables, we thus consider the following problem: Find $((\boldsymbol{u}_\mathcal{T}, p_\mathcal{T}), (\boldsymbol{u}_\mathcal{F}, p_\mathcal{F}), (\boldsymbol{y}_\mathcal{C}, y_\mathcal{C}), \boldsymbol{y}_\mathcal{D}) \in (\boldsymbol{\mathcal{H}}_\mathcal{T} \times \mathcal{H}_\mathcal{T}) \times (\boldsymbol{\mathcal{H}}_\mathcal{F} \times \mathcal{H}_\mathcal{F}) \times (\boldsymbol{\mathcal{H}}_\mathcal{C} \times \mathcal{H}_\mathcal{C}) \times (\boldsymbol{\mathcal{H}}_\mathcal{D} \times \mathcal{H}_\mathcal{D})$ such that we have the following problems.

Coarse problem.

$$a_\mathcal{D}(\{\boldsymbol{u}_\mathcal{T}, \boldsymbol{u}_\mathcal{F}\}, \boldsymbol{v}) = -\int_\Omega \boldsymbol{f}_{\boldsymbol{u}} \cdot \boldsymbol{v}\, d\boldsymbol{x} \qquad \text{for all } \boldsymbol{v} \in \boldsymbol{\mathcal{H}}_\mathcal{T}, \tag{22}$$

$$\begin{aligned} &b_{\mathcal{D},1}(\{\boldsymbol{u}_\mathcal{T}, \boldsymbol{u}_\mathcal{F}\}, r) - [\rho_\mathcal{T} p_\mathcal{T}, r]_{\mathcal{T},0} \\ &\quad - \tau c_\mathcal{D}(\{p_\mathcal{T}, p_\mathcal{F}\}, r) = -\int_\Omega f_p \cdot r\, d\boldsymbol{x} \qquad \text{for all } r \in \mathcal{H}_\mathcal{T}. \end{aligned} \tag{23}$$

Fine problems.

$$\begin{aligned} &a_\mathcal{D}(\{\boldsymbol{0}, \boldsymbol{u}_\mathcal{F}\}, \boldsymbol{v}) \\ &\quad = -a_\mathcal{D}(\{\boldsymbol{u}_\mathcal{T}, \boldsymbol{0}\}, \boldsymbol{v}) - b_{\mathcal{D},2}^T(\{p_\mathcal{T}, 0\}, \boldsymbol{v}) \qquad \text{for all } \boldsymbol{v} \in \boldsymbol{\mathcal{H}}_\mathcal{F} \cap \boldsymbol{\mathcal{H}}_\mathcal{C}, \end{aligned} \tag{24}$$

$$c_{\mathcal{D}}(\{0,p_{\mathcal{F}}\},r) = -c_{\mathcal{D}}(\{p_{\mathcal{T}},0\},r) \qquad \text{for all } r \in \mathcal{H}_{\mathcal{F}} \cap \mathcal{H}_{\mathcal{C}}, \tag{25}$$

$$\begin{aligned} &d_{\mathcal{D}}\big((\{\mathbf{0},\boldsymbol{u}_{\mathcal{F}}\},\{0,p_{\mathcal{F}}\}),\boldsymbol{w}\big) \\ &\qquad = -d_{\mathcal{D}}\big((\{\boldsymbol{u}_{\mathcal{T}},\mathbf{0}\},\{p_{\mathcal{T}},0\}),\boldsymbol{w}\big) \qquad \text{for all } \boldsymbol{w} \in (\boldsymbol{\mathcal{H}}_{\mathcal{D}} \times \mathcal{H}_{\mathcal{D}}), \end{aligned} \tag{26}$$

$$\begin{aligned} &e_{\mathcal{D}}\big((\{\mathbf{0},\boldsymbol{u}_{\mathcal{F}}\},\{0,p_{\mathcal{F}}\}),(\boldsymbol{w},w)\big) + \hat{a}_{\mathcal{D}}(\boldsymbol{w},\boldsymbol{y}_{\mathcal{C}}) \\ &\quad + b_{\mathcal{D}}(\boldsymbol{w},y_{\mathcal{C}}) + b_{\mathcal{D}}^{T}(w,\boldsymbol{y}_{\mathcal{C}}) \\ &\quad - c(w,y_{\mathcal{C}}) + d_{\mathcal{D}}\big((\boldsymbol{w},w),\boldsymbol{y}_{\mathcal{D}}\big) \\ &\qquad = -e_{\mathcal{D}}\big((\{\boldsymbol{u}_{\mathcal{T}},\mathbf{0}\},\{p_{\mathcal{T}},0\}),(\boldsymbol{w},w)\big) \qquad \text{for all } (\boldsymbol{w},w) \in (\boldsymbol{\mathcal{H}}_{\mathcal{D}} \times \mathcal{H}_{\mathcal{D}}). \end{aligned} \tag{27}$$

In the above equations, we have abused notation slightly be letting "0" represent elements in either spaces $\mathcal{H}_{\mathcal{T}}$ or $\mathcal{H}_{\mathcal{F}}$; however, the meaning should be clear from the context. Furthermore, we note the following important details which arise as a consequence of the previous definitions: There is no coupling term in the coarse equation (22) since by Gauss's theorem, $b_{\mathcal{D},2}^{T}(p_{\mathcal{D}},\boldsymbol{v}) = 0$ for all $\boldsymbol{v} \in \boldsymbol{\mathcal{H}}_{\mathcal{T}}$. Similarly, by the definition in (16), there are no coupling terms $b_{\mathcal{D},1}$ in (25), and only the coarse component appears in (24). Finally, there is no source term on the right-hand side of (24) and (25) since $\Pi_{\mathcal{T}}(\mathcal{H}_{\mathcal{F}} \cap \mathcal{H}_{\mathcal{C}}) = 0$.

The discrete VMS formulation given above allows us to define a fine-scale interpolation operator for the FV method: $\Pi_{FV} : \boldsymbol{\mathcal{H}}_{\mathcal{T}} \times \mathcal{H}_{\mathcal{T}} \to \boldsymbol{\mathcal{H}}_{\mathcal{D}} \times \mathcal{H}_{\mathcal{D}}$. Furthermore, due to the lack of coupling terms in (25) and the linearity of the system, we note that this interpolation operator can be decomposed as

$$\Pi_{FV}\{\boldsymbol{u}_{\mathcal{T}},p_{\mathcal{T}}\} = \{\Pi_{FV}^{\boldsymbol{u},\boldsymbol{u}}\boldsymbol{u}_{\mathcal{T}} + \Pi_{FV}^{\boldsymbol{u},p}p_{\mathcal{T}}, \Pi_{FV}^{p}p_{\mathcal{T}}\}. \tag{28}$$

Here the fluid interpolation operator Π_{FV}^{p} is (due to the lack of coupling in (25)) identical to the standard operator for the uncoupled system. In MPFA terminology this is the solution operator for the interaction region problem [1]. Similarly, and again due to linearity, it is easily verified that the solid operator $\Pi_{FV}^{\boldsymbol{u},\boldsymbol{u}}$ is also identical to the FV interpolation operator for the uncoupled problem [29]. The critical novel component is the influence of the cell-centered pressures on the subscale structure of the displacement, given by $\Pi_{FV}^{\boldsymbol{u},p}$. We will find below that *this operator is essential for the consistency and stability of the method* and would be neglected if simply introducing the Biot coupling at the coarse scale [28].

The following lemma establishes the computational applicability of the method.

LEMMA 9. *The FV interpolation Π_{FV} is local, in the sense that it can be decomposed as*

$$\Pi_{FV} = \sum_{s\in\mathcal{V}} \Pi_{FV,s}, \tag{29}$$

where, furthermore, for each $s \in \mathcal{V}$, the operator $\Pi_{FV,s}$ depends only on elements in $\boldsymbol{\mathcal{H}}_{\mathcal{T}_s} \times \mathcal{H}_{\mathcal{T}_s}$.

Proof. Let $\chi_{\mathcal{D}}$ be any of the bilinear forms defined in (13)–(18). We note that in all definitions the sums can be rearranged such that

$$\chi_{\mathcal{D}} = \sum_{s\in\mathcal{V}} \chi_{\mathcal{D},s}. \tag{30}$$

By inspection, we see that all bilinear forms $\chi_{\mathcal{D},s}$ have local support, involving only elements in $\boldsymbol{\mathcal{H}}_{\mathcal{T}_s} \times \mathcal{H}_{\mathcal{T}_s}$ and variables $(\boldsymbol{u},p)_{K,s'}^{\sigma,\beta} \in \boldsymbol{\mathcal{H}}_{\mathcal{F}} \times \mathcal{H}_{\mathcal{F}}$ with $s' = s$. Hence, the local systems (24)–(27) form a block-diagonal system with respect to $\boldsymbol{\mathcal{H}}_{\mathcal{F}} \times \mathcal{H}_{\mathcal{F}}$ and can be solved locally for each vertex. ◻

Lemma 10. *The local systems given by* (24)–(27) *have a unique solution* $(\boldsymbol{u}_{\mathcal{F}}, p_{\mathcal{F}}) \in (\boldsymbol{\mathcal{H}}_{\mathcal{F}} \times \mathcal{H}_{\mathcal{F}})$ *for each* $(\boldsymbol{u}_{\mathcal{T}}, p_{\mathcal{T}}) \in \boldsymbol{\mathcal{H}}_{\mathcal{T}} \times \mathcal{H}_{\mathcal{T}}$.

Proof. The unique solvability for both the fluid and the solid problems follows from coercivity arguments as given in [29]. ◻

The existence and uniqueness of the solution define the locally computable FV interpolations Π_{FV}, and thus we define the following.

Definition 11. *For every* $s \in \mathcal{V}$*, the local mixed problem* (24)–(27) *has a unique solution by Lemma* 10*, and we define the norm of the of the solution operator* $\Pi_{FV,s}$ *as* $\theta_{1,s}$ *such that for all* $(\boldsymbol{u}, p) \in (\boldsymbol{\mathcal{H}}_{\mathcal{T}} \times \mathcal{H}_{\mathcal{T}})$,

$$\|\Pi^{\boldsymbol{u},\boldsymbol{u}}_{FV,s}\boldsymbol{u}\|_{\mathcal{D},s} + h^{-1}\|\Pi^{\boldsymbol{u},p}_{FV,s}p\|_{\mathcal{D},s} + \|\Pi^{p}_{FV,s}p\|_{\mathcal{D},s} \le \theta_{1,s}(\|\boldsymbol{u}\|_{\mathcal{T},s} + \|p\|_{\mathcal{T},s}). \tag{31}$$

It follows from the definition of norms and the scaling invariance of (24)–(27) that the constants θ may depend on heterogeneity and grid geometry but not on domain size or mesh size. In particular, the appearance of h^{-1} is due to the lack of a derivative on $p_{\mathcal{D}}$ in the bilinear form $b^{T}_{\mathcal{D},2}$ in (24).

4.2. Cell-centered discretization for Biot's equations.

We are now prepared to state the cell-centered discretization of Biot's equations. Indeed, by replacing the fine-scale terms in (22)–(23) by the FV interpolation Π_{FV}, we obtain a finite cell-centered FV discretization. From section 4.1 we thus obtain the following coarse problem: Find $(\boldsymbol{u}_{\mathcal{T}}, p_{\mathcal{T}}) \in \boldsymbol{\mathcal{H}}_{\mathcal{T}} \times \mathcal{H}_{\mathcal{T}}$ such that

$$a_{\mathcal{D}}(\Pi^{\boldsymbol{u},\boldsymbol{u}}_{FV}\boldsymbol{u}_{\mathcal{T}}, \boldsymbol{v}) + a_{\mathcal{D}}(\Pi^{\boldsymbol{u},p}_{FV}p_{\mathcal{T}}, \boldsymbol{v}) = -\int_{\Omega} \boldsymbol{f}_{\boldsymbol{u}} \cdot \boldsymbol{v}\, d\boldsymbol{x} \qquad \text{for all } \boldsymbol{v} \in \boldsymbol{\mathcal{H}}_{\mathcal{T}}, \tag{32}$$

$$\begin{aligned} &b_{\mathcal{D},1}(\Pi^{\boldsymbol{u},\boldsymbol{u}}_{FV}\boldsymbol{u}_{\mathcal{T}}, r) - [\rho_{\mathcal{T}} p_{\mathcal{T}}, r]_{\mathcal{T},0} \\ &\qquad - \tau c_{\mathcal{D}}(\Pi^{p}_{FV}p_{\mathcal{T}}, r) + b_{\mathcal{D},1}(\Pi^{\boldsymbol{u},p}_{FV}p_{\mathcal{T}}, r) = -\int_{\Omega} f_p \cdot r\, d\boldsymbol{x} \quad \text{for all } r \in \mathcal{H}_{\mathcal{T}}. \end{aligned} \tag{33}$$

Importantly, in (32)–(33), two nonstandard terms have appeared due to the coupling between fluid pressure and deformation captured by $\Pi^{\boldsymbol{u},p}_{FV}$. The term $a_{\mathcal{D}}(\Pi^{\boldsymbol{u},p}_{FV}p_{\mathcal{T}}, \boldsymbol{v})$ in (32) will be seen as an approximation of the continuous operator $(p, \nabla \cdot \boldsymbol{v})$ and thus provides the correct impact of pressure in the mechanical equation. In contrast, the term $b_{\mathcal{D},1}(\Pi^{\boldsymbol{u},p}_{FV}p_{\mathcal{T}}, r)$ in (33) is a local consistency operator which approximates the subscale impact of pressure gradients on local volume changes.

For convenience of notation, we will define by capital letters the bilinear forms with the FV interpolations suppressed, such that, e.g., $A_{\mathcal{D}}(\boldsymbol{u}_{\mathcal{T}}, \boldsymbol{v}) = a_{\mathcal{D}}(\Pi^{\boldsymbol{u},\boldsymbol{u}}_{FV}\boldsymbol{u}_{\mathcal{T}}, \boldsymbol{v})$. The exceptions to this rule are the coupling term, which for notational consistency is denoted by $B^{T}_{\mathcal{D},2} = a_{\mathcal{D}}(\Pi^{\boldsymbol{u},p}_{FV}p_{\mathcal{T}}, \boldsymbol{v})$, and the local consistency operator, which is denoted by $\Delta_{\mathcal{D}}(p_{\mathcal{T}}, r) = b_{\mathcal{D}}(\Pi^{\boldsymbol{u},p}_{FV}p_{\mathcal{T}}, r)$. This allows us to define our cell-centered discretizations compactly.

Definition 12. *We then refer to the following system as the* MPSA/MPFA-FV discretization *for Biot's equations: Find* $(\boldsymbol{u}_{\mathcal{T}}, p_{\mathcal{T}}) \in \boldsymbol{\mathcal{H}}_{\mathcal{T}} \times \mathcal{H}_{\mathcal{T}}$ *such that*

$$A_{\mathcal{D}}(\boldsymbol{u}_{\mathcal{T}}, \boldsymbol{v}) + B^{T}_{\mathcal{D},2}(p_{\mathcal{T}}, \boldsymbol{v}) = -\int_{\Omega} \boldsymbol{f}_{\boldsymbol{u}} \cdot \boldsymbol{v}\, dx \qquad \textit{for all } \boldsymbol{v} \in \boldsymbol{\mathcal{H}}_{\mathcal{T}}, \tag{34}$$

$$B_{\mathcal{D},1}(\boldsymbol{u}_{\mathcal{T}}, r) - [\rho_{\mathcal{T}} p_{\mathcal{T}}, r]_{\mathcal{T},0} \tag{35}$$

$$-\tau C_{\mathcal{D}}(p_{\mathcal{T}}, r) + \Delta_{\mathcal{D}}(p_{\mathcal{T}}, r) = -\int_\Omega f_p \cdot r \, d\boldsymbol{x} \quad \textit{for all } r \in \mathcal{H}_{\mathcal{T}}.$$

We will refer to this system in shorthand as

$$\mathfrak{A}_{\mathcal{D}}(\boldsymbol{u}_{\mathcal{T}}, p_{\mathcal{T}}, \boldsymbol{v}, r) = \mathfrak{B}(\boldsymbol{v}, r) \quad \textit{for all } (\boldsymbol{v}, r) \in \boldsymbol{\mathcal{H}}_{\mathcal{T}} \times \mathcal{H}_{\mathcal{T}}, \tag{36}$$

where to be precise, we may sometimes explicitly include the parameter dependencies in the bilinear form, $\mathfrak{A}_{\mathcal{D}} = \mathfrak{A}_{\mathcal{D}}(\boldsymbol{u}_{\mathcal{T}}, p_{\mathcal{T}}, \boldsymbol{v}, r; \rho, \tau)$.

Remark 13. Because of the static condensation, the *local consistency operator* $\Delta_{\mathcal{D}}(p_{\mathcal{T}}, r)$ has appeared in the fluid pressure system. Since $\Pi_{FV}^{\boldsymbol{u},p} p_{\mathcal{T}}$ expresses a displacement response to pressure and $b_{\mathcal{D},2}$ evaluates the discrete divergence, and by scaling arguments, we qualitatively identify the new term as proportional to a weak discretization of $h^2 \frac{\partial}{\partial t} \nabla \cdot (\alpha \kappa^{-1} \nabla(\alpha p))$, where κ is the bulk modulus of the material. Terms with similar scaling have previously been introduced artificially in order to obtain a stable discretization of equations (1) (see, e.g., [11, 16]). We note that this term is essential for the stability method of the current scheme, although numerical experiments indicate that it is not sufficient to guarantee monotonicity of the resulting pressure solution.

Remark 14. For analysis, it will be desirable to control the asymmetry of the coupling terms. However, we note that this is not possible on the current form since $B_{\mathcal{D},1}(\boldsymbol{u}_{\mathcal{T}}, r) \sim \|\boldsymbol{u}_{\mathcal{T}}\|_{\mathcal{T}} \|r\|_{\mathcal{T},0}$ while $B_{\mathcal{D},2}^T(p_{\mathcal{T}}, \boldsymbol{v}) \sim \|p_{\mathcal{T}}\|_{\mathcal{T}} \|\boldsymbol{v}\|_{\mathcal{T},0}$. However, we exploit (24) to obtain the relationship that for all $(\boldsymbol{v}, p_{\mathcal{T}}) \in \boldsymbol{\mathcal{H}}_{\mathcal{T}} \times \mathcal{H}_{\mathcal{T}}$,

$$\begin{aligned} a_{\mathcal{D}}(\Pi_{FV}^{\boldsymbol{u},p} p_{\mathcal{T}}, \boldsymbol{v}) &= a_{\mathcal{D}}(\Pi_{FV}^{\boldsymbol{u},p} p_{\mathcal{T}}, \Pi_{\mathcal{T}} \Pi_{FV}^{\boldsymbol{u},\boldsymbol{u}} \boldsymbol{v}) \\ &= a_{\mathcal{D}}(\Pi_{FV}^{\boldsymbol{u},p} p_{\mathcal{T}}, \Pi_{\mathcal{C}} \Pi_{FV}^{\boldsymbol{u},\boldsymbol{u}} \boldsymbol{v}) + b_{\mathcal{D},2}^T(p_{\mathcal{T}}, \Pi_{\mathcal{C}} \Pi_{FV}^{\boldsymbol{u},\boldsymbol{u}} \boldsymbol{v}). \end{aligned} \tag{37}$$

Then, by the definition of the bilinear forms, we have that

$$\begin{aligned} B_{\mathcal{D},2}^T(p_{\mathcal{T}}, \boldsymbol{v}) = B_{\mathcal{D},1}^T(p_{\mathcal{T}}, \boldsymbol{v}) &+ a_{\mathcal{D}}(\Pi_{FV}^{\boldsymbol{u},p} p_{\mathcal{T}}, \Pi_{\mathcal{C}} \Pi_{FV}^{\boldsymbol{u},\boldsymbol{u}} \boldsymbol{v}) \\ &+ [b_{\mathcal{D},2}^T(p_{\mathcal{T}}, \Pi_{\mathcal{C}} \Pi_{FV}^{\boldsymbol{u},\boldsymbol{u}} \boldsymbol{v}) - b_{\mathcal{D},1}(\Pi_{FV}^{\boldsymbol{u},\boldsymbol{u}} \boldsymbol{v}, p_{\mathcal{T}})]. \end{aligned} \tag{38}$$

In what follows, we will denote the asymmetric terms as

$$\Lambda_{\mathcal{D}}(p_{\mathcal{T}}, \boldsymbol{v}) = a_{\mathcal{D}}(\Pi_{FV}^{\boldsymbol{u},p} p_{\mathcal{T}}, \Pi_{\mathcal{C}} \Pi_{FV}^{\boldsymbol{u},\boldsymbol{u}} \boldsymbol{v}) + [b_{\mathcal{D},2}^T(p_{\mathcal{T}}, \Pi_{\mathcal{C}} \Pi_{FV}^{\boldsymbol{u},\boldsymbol{u}} \boldsymbol{v}) - b_{\mathcal{D},1}(\Pi_{FV}^{\boldsymbol{u},\boldsymbol{u}} \boldsymbol{v}, p_{\mathcal{T}})] \tag{39}$$

such that (34) can be equivalently written as

$$A_{\mathcal{D}}(\boldsymbol{u}_{\mathcal{T}}, \boldsymbol{v}) + B_{\mathcal{D},1}^T(p_{\mathcal{T}}, \boldsymbol{v}) + \Lambda_{\mathcal{D}}(p_{\mathcal{T}}, \boldsymbol{v}) = -\int_\Omega \boldsymbol{f}_{\boldsymbol{u}} \cdot \boldsymbol{v} \, d\boldsymbol{x} \quad \text{for all } \boldsymbol{v} \in \boldsymbol{\mathcal{H}}_{\mathcal{T}}. \tag{40}$$

While (34) and (40) are formally identical, we note that due to the conservation structure, (34)–(35) are natural from the perspective of method formulation and implementation. Conversely, as $\Lambda_{\mathcal{D}}(p_{\mathcal{T}}, \boldsymbol{v})$ can be bounded by scaling arguments as seen below, (35) and (40) are more convenient for analysis.

5. Convergence.

In the introduction, we noted that the two main concerns for discretizing the Biot equations are stability with respect to incompressible materials, as well as small time-steps, which is represented Definition 1. In this section, we will show stability and convergence of the discretization, independent of small parameters, dependent only on locally computable conditions on the grid.

5.1. Stability of uncoupled problems. It is well known that FV methods of the type considered herein are stable and convergent for a wide range of grids [21, 3, 13]. In particular, we will make use of the following mild local condition on the mesh and parameters.

Condition A. For every vertex $s \in \mathcal{V}$, there exists a constant $\theta_s^c \geq \theta^c > 0$ such that the bilinear form $c_{\mathcal{D},s}$ and the interpolation $\Pi_{FV,s}^p$ satisfy that for all $p \in \Pi_{FV,s}^p \mathcal{H}_\mathcal{T}$,

$$c_{\mathcal{D},s}(p, \Pi_\mathcal{C} p) \geq \theta_s^c \left(|p|^2_{c_{\mathcal{D},s}} + \sum_{K \in \mathcal{T}_s} \sum_{\sigma \in \mathcal{F}_s \cap \mathcal{F}_K} \frac{m_K^s}{d_{K,\sigma}^2} \frac{1}{m_s^\sigma} \sum_{\beta \in \mathcal{G}_s^\sigma} \omega_\beta \big([[p]]_s^{\sigma,\beta} \big)^2 \right), \tag{41}$$

where the local energy seminorm is associated with the symmetrized bilinear form

$$|p|^2_{c_{\mathcal{D},s}} = \sum_{K \in \mathcal{T}_s} m_K^s k_K ((\overline{\nabla} p)_K^s)^2.$$

For the solid deformation problem, a similar local coercivity condition is needed.

Condition B. For every vertex $s \in \mathcal{V}$, there exists a constant $\theta_s^a \geq \theta^a > 0$ such that the bilinear form $a_{\mathcal{D},s}$ and the interpolation $\Pi_{FV,s}^{\boldsymbol{u},\boldsymbol{u}}$ satisfy that for all $\boldsymbol{u} \in \Pi_{FV,s}^{\boldsymbol{u},\boldsymbol{u}} \boldsymbol{\mathcal{H}}_\mathcal{T}$,

$$a_{\mathcal{D},s}(\boldsymbol{u}, \Pi_\mathcal{C} \boldsymbol{u}) \geq \theta_s^a \left(|\boldsymbol{u}|^2_{a_{\mathcal{D},s}} + \sum_{K \in \mathcal{T}_s} \sum_{\sigma \in \mathcal{F}_s \cap \mathcal{F}_K} \frac{m_K^s}{d_{K,\sigma}^2} \frac{1}{m_s^\sigma} \sum_{\beta \in \mathcal{G}_s^\sigma} \omega_\beta \big([[\boldsymbol{u}]]_s^{\sigma,\beta} \big)^2 \right), \tag{42}$$

where the local energy seminorm is associated with the symmetrized bilinear form

$$|\boldsymbol{u}|^2_{a_{\mathcal{D},s}} = \sum_{K \in \mathcal{T}_s} m_K^s (\overline{\nabla} \boldsymbol{u})_K^s : \mathbb{C} : (\overline{\nabla} \boldsymbol{u})_K^s.$$

Conditions A and B are in practice a condition on the grid regularity and the structure (but not magnitude) of the material properties. These conditions can be verified locally while assembling the discretization, and moreover they can be verified a priori for certain classes of meshes [29].

The known stability results are recalled in the following lemma (see [3, 29]).

LEMMA 15. *For given parameter fields* $\mathbb{C}$ *and mesh* $\mathcal{D}$, *let Conditions* A *and* B *hold. Then the bilinear forms* $A_\mathcal{D}$ *and* $C_\mathcal{D}$ *are coercive and for all* $\boldsymbol{u} \in \boldsymbol{\mathcal{H}}_\mathcal{T}$ *and* $p \in \mathcal{H}_\mathcal{T}$ *there exist positive constants* Θ^A *and* Θ^C *such that*

$$A_\mathcal{D}(\boldsymbol{u}, \boldsymbol{u}) \geq \Theta^A \|\boldsymbol{u}\|^2_\mathcal{T} \quad \text{and} \quad (\rho_\mathcal{T} p, p) + \tau C_\mathcal{D}(p, p) \geq \rho \|p\|^2_{\mathcal{T},0} + \tau \Theta^C \|p\|^2_\mathcal{T}. \tag{43}$$

The constants Θ^A and Θ^C are dependent on the parameters of the problem and the mesh triplet $\mathcal{D}$ through the constants θ^a and θ^c, but they do not scale with h. Here, and in what follows, we will use the convention on material parameters from section 1 such that $\rho = \sup_{K \in \mathcal{T}} \rho_K$.

5.2. Properties of the nonstandard terms. To proceed, we will need to verify that the local consistency operator $\Delta_\mathcal{D}$ is stable and identify a bound on the properties of $\Lambda_\mathcal{D}$. We first identify a local coercivity condition on the mesh similar to those stated above.

Condition C. For every internal vertex $s \in \mathcal{V}$ with an associated local mesh diameter $h_s = \max_{K\in\mathcal{T}_s} d_K$, there exists a constant $\theta_s^\Delta \geq \theta^\Delta > 0$ such that the bilinear form $b_{\mathcal{D},s}$ and the interpolation $\Pi_{FV,s}^{\boldsymbol{u},p}$ satisfy that for all $p \in \mathcal{H}_\mathcal{T}$,

$$b_{\mathcal{D},s}(\Pi_{FV,s}^{\boldsymbol{u},p} p, p) \geq h_s^2 \theta_s^\Delta \left(|p|^2_{\Delta_{\mathcal{D},s}} + \sum_{K\in\mathcal{T}_s} \sum_{\sigma\in\mathcal{F}_s\cap\mathcal{F}_K} \frac{m_K^s}{d_{K,\sigma}^2} \frac{1}{m_s^\sigma} \sum_{\beta\in\mathcal{G}_s^\sigma} \omega_\beta \left([[p]]_s^{\sigma,\beta} \right)^2 \right), \tag{44}$$

where the local energy seminorm is associated with the symmetrized bilinear form

$$|p|^2_{\Delta_{\mathcal{D},s}} = \sum_{K\in\mathcal{T}_s} m_K^s ((\overline{\nabla} p)_K^s)^2.$$

As with Conditions A and B, the local structure of Condition C allows it to be easily verified a priori for grids with local symmetry using arguments similar to those found in [29], and it can be verified numerically at the discretization stage for arbitrary grids. The structure of this condition, and in particular the scaling h_s^2, follows from (31) and the relationship between the norms.

LEMMA 16. *For given parameter fields $\mathbb{C}$ and mesh $\mathcal{D}$, let Condition* C *hold; then the bilinear form $\Delta_\mathcal{D}$ is coercive and for all $p \in \mathcal{H}_\mathcal{T}$ there exists a positive constant Θ^Δ such that*

$$\Delta_\mathcal{D}(p,p) \leq -h^2 \Theta^\Delta |p|^2_\mathcal{T}. \tag{45}$$

The constant Θ^Δ is dependent on the mesh triplet $\mathcal{D}$ through the constant θ^Δ, but it does not scale with h.

Proof. The lemma follows by summation of (44), the well-posedness of the local problems, and scaling arguments. Note that we do not get a full norm since $\Pi_{FV}^{\boldsymbol{u},p} p_\mathcal{T}$ does not depend on the Dirichlet boundary data on $\Gamma_{p,D}$. ☐

Finally, we bound the nonsymmetric part of the coupling.

DEFINITION 17. *For every vertex $s \in \mathcal{V}$ with an associated local mesh diameter $h_s = \max_{K\in\mathcal{T}_s} d_K$, there exist two constants $\theta_1^\Lambda \geq \theta_{1,s}^\Lambda > 0$ and $\theta_2^\Lambda \geq \theta_{2,s}^\Lambda > 0$ such that the bilinear form $b_{\mathcal{D},s}$ and the interpolation $\Pi_{FV,s}^{\boldsymbol{u},p}$ satisfy that for all $p \in \mathcal{H}_\mathcal{T}$,*

$$a_{\mathcal{D},s}(\Pi_{FV}^{\boldsymbol{u},p} p_\mathcal{T}, \Pi_\mathcal{C} \Pi_{FV}^{\boldsymbol{u},\boldsymbol{u}} \boldsymbol{v}) \geq -h_s \theta_{1,s}^\Lambda |p|_{\mathcal{T},s} \|\boldsymbol{v}\|_{\mathcal{T},s} \tag{46}$$

and

$$\left[b_{\mathcal{D},2,s}^T (p_\mathcal{T}, \Pi_\mathcal{C} \Pi_{FV}^{\boldsymbol{u},\boldsymbol{u}} \boldsymbol{v}) - b_{\mathcal{D},1,s}(\Pi_{FV}^{\boldsymbol{u},\boldsymbol{u}} \boldsymbol{v}, p_\mathcal{T}) \right] \geq -\theta_{2,s}^\Lambda \|p\|_{\mathcal{T},0,s} \|\boldsymbol{v}\|_{\mathcal{T},s}. \tag{47}$$

We note that the existence of these constants follows from scaling arguments and the linearity of the introduced operators.

LEMMA 18. *There exists a lower bound on the bilinear forms $\Lambda_\mathcal{D}$ denoted by Θ^Λ such that the following inequality holds:*

$$\Lambda_\mathcal{D}(\boldsymbol{v}, p) \geq -\Theta^\Lambda \|p\|_{\mathcal{T},0} \|\boldsymbol{v}\|_\mathcal{T} \quad \text{for all } p \in \mathcal{H}_\mathcal{T} \text{ and } \boldsymbol{v} \in \boldsymbol{\mathcal{H}}_\mathcal{T}. \tag{48}$$

Furthermore, the constant $\Theta^\Lambda \leq \max(d^{-1/2}\theta_1^\Lambda, \theta_2^\Lambda)$.

Proof. To show (48), we start from the definition of the bilinear form, and by the triangle inequality we have that

$$\Lambda_\mathcal{D}(\boldsymbol{v}, p) = \sum_{s\in\mathcal{V}} a_{\mathcal{D},s}(\Pi_{FV}^{\boldsymbol{u},p} p_\mathcal{T}, \Pi_\mathcal{C} \Pi_{FV}^{\boldsymbol{u},\boldsymbol{u}} \boldsymbol{v}) + \left[b_{\mathcal{D},2,s}^T (p_\mathcal{T}, \Pi_\mathcal{C} \Pi_{FV}^{\boldsymbol{u},\boldsymbol{u}} \boldsymbol{v}) - b_{\mathcal{D},1,s}(\Pi_{FV}^{\boldsymbol{u},\boldsymbol{u}} \boldsymbol{v}, p_\mathcal{T}) \right]$$

$$\geq -\sum_{s\in\mathcal{V}}\left[h_s\theta^{\Lambda}_{1,s}|p|_{\mathcal{T},s}\|\boldsymbol{v}\|_{\mathcal{T},s}+\theta^{\Lambda}_{2,s}\|p\|_{\mathcal{T},s,0}\|\boldsymbol{v}\|_{\mathcal{T},s}\right]$$
$$\geq -\Theta^{\Lambda}\|p\|_{\mathcal{T},0}\|\boldsymbol{v}\|_{\mathcal{T}}.$$

Here the last inequality uses the inverse inequality stated in section 2. ☐

5.3. Stability of coupled system. Let us first note that the simplest approaches to showing the stability of the coupled system are not adequate. Indeed, from (35) and (40), we immediately obtain a stability estimate for the coupled problem based on Lemmas 15, 16, and 18, e.g.,

$$\mathfrak{A}_{\mathcal{D}}(\boldsymbol{u},p,\boldsymbol{u},-p)\geq \Theta^{A}\|\boldsymbol{u}\|^2_{\mathcal{T}}+\tau\Theta^{C}\|p\|^2_{\mathcal{T}} + h^2\Theta^{\Delta}|p|^2_{\mathcal{T}}+\rho\|p\|^2_{\mathcal{T},0}-\Theta^{\Lambda}\|p\|_{\mathcal{T},0}\|\boldsymbol{u}\|_{\mathcal{T},0}. \tag{49}$$

This estimate is unsatisfactory, as it contains a negative term, and furthermore there is no bound on pressure as $\rho,\tau,h\to 0$. To remedy this situation, we must explicitly utilize the properties of the coupling term $B_{\mathcal{D},1}$, which is usually achieved through showing that an inf-sup condition holds [11]. In our case, however, this is not possible; the kernel of $B_{\mathcal{D},1}$ admits nontrivial oscillatory solutions. The most notable example arises on square grids, where if the pressure p is a so-called checker-board pattern, then $B_{\mathcal{D},1}(p,\boldsymbol{v})=0$ for all $\boldsymbol{v}\in\boldsymbol{\mathcal{H}}_{\mathcal{D}}$. This is a fundamental consequence of Galilean invariance of the discretization and is common for all low-order discretizations with co-located variables [11, 24].

To prove stability of the system, we must therefore exploit the structure of the full coupled system. Intuitively, the observation that nonoscillatory solutions are well captured by $B_{\mathcal{D},1}(p,\boldsymbol{v})$, while oscillatory solutions have a more favorable bound than that given in Lemma 15, allows us to expect that the presence of the local consistency operator, which we have qualitatively identified as a Laplacian-like term, proportional to h^2, may be sufficient to stabilize the system. Indeed, this is the idea behind several stabilization techniques, and as applied to finite element discretizations for Stokes [12] as well as finite element [8] and finite difference [17] discretizations of Biot's equation. The main difference between the cited works and the present is that in previous work a stabilization was introduced explicitly or through augmented formulations; herein the term arises as a natural part of the discretization.

To prove that the system $\mathfrak{A}_{\mathcal{D}}$ is indeed stable, our analysis will follow a path similar to that of Franca and Stenberg, who analyzed finite element discretizations of augmented formulations for mixed forms of the elasticity equations [15]. The main idea is to use the properties of $B_{\mathcal{D},1}$ to trade the $|p|^2_{\mathcal{T}}$ term in (49) for a deficiency in the inf-sup condition. Thus we do not have an inf-sup condition in the sense of Brezzi [10] but rather derive inf-sup for the global system in the sense of Babuska [7]. We will need some technical results. In the following, C and c represent generic positive constants, independent of h.

Let us first introduce an interpolation operator from the discrete to continuous setting, in the spirit of a discontinuous Galerkin interpretation.

Definition 19. *Let the interpolation operator* $\Pi_{L^2}\colon\boldsymbol{\mathcal{H}}_{\mathcal{D}}\to(L^2(\Omega))^d$ *be defined such that for all* $(K,s)\in\mathcal{T}\times\mathcal{V}$ *and* $\boldsymbol{x}\in K$, *we have* $\Pi_{L^2}\boldsymbol{u}(\boldsymbol{x})=\boldsymbol{u}_K+(\overline{\nabla}\boldsymbol{u})^s_K\cdot(\boldsymbol{x}-\boldsymbol{x}_K)$.

Lemma 20. *For all* $p\in\mathcal{H}_{\mathcal{T}}$, *it holds that*

$$\sup_{\boldsymbol{w}\in\boldsymbol{H}^1}\frac{(p,\nabla\cdot\boldsymbol{w})}{\|\boldsymbol{w}\|_1}\geq c_{LBB}\|p\|_{\mathcal{T},0}.$$

Proof. Since $\mathcal{H}_\mathcal{T} \in L^2$, the result follows from the well-posedness of the continuous problem, and the constant c_{LBB} is no worse than the inf-sup constant for the continuous problem. ∎

LEMMA 21. *For all* $\boldsymbol{w} \in \boldsymbol{H}^1$, *there exists* $\widetilde{\boldsymbol{w}} \in \boldsymbol{\mathcal{H}}_\mathcal{T}$ *such that*

$$\|\widetilde{\boldsymbol{w}}\|_\mathcal{T} \leq \|\boldsymbol{w}\|_1$$

and

$$\|\Pi_\mathcal{D}\boldsymbol{w} - \Pi_{FV}^{\boldsymbol{u},\boldsymbol{u}}\widetilde{\boldsymbol{w}}\|_{\mathcal{D},0} \leq ch\|\boldsymbol{w}\|_1.$$

Proof. The result follows from the stability of the local calculations (Lemma 10 and Definition 11) and scaling arguments [21, 14]. ∎

We now consider the following weakened LBB-type condition, the proof of which closely follows the approach used in [15] but is adapted to the discrete norms used herein and the finite spaces $\Pi_{L^2}\Pi_{FV}^{\boldsymbol{u},\boldsymbol{u}}\boldsymbol{\mathcal{H}}_\mathcal{T}$.

LEMMA 22. *For sufficiently fine grids, the bilinear form* $B_{\mathcal{D},1}$ *satisfies*

$$\sup_{\substack{\boldsymbol{v}\in\boldsymbol{\mathcal{H}}_\mathcal{T}\\ \|\boldsymbol{v}\|_\mathcal{T}=1}} B_{\mathcal{D},1}(\boldsymbol{v},p) \geq \Theta^B|p|_{\mathcal{T},0} - \theta^B h|p|_\mathcal{T} \quad \text{for all } p \in \mathcal{H}_\mathcal{T}. \tag{50}$$

Proof. Now for any $p \in \mathcal{H}_\mathcal{T}$, consider the splitting such that $p = \bar{p} + \widetilde{p}$, where $\bar{p} = |\Omega|^{-1}\sum_{K\in\mathcal{T}} m_K p_K$. Then by Lemma 20 there exists $\boldsymbol{w} \in \boldsymbol{\mathcal{H}}_0^1$ such that

$$(\nabla\cdot\boldsymbol{w},\widetilde{p}) \geq c_{LBB}\|\widetilde{p}\|_{\mathcal{T},0}\|\boldsymbol{w}\|_1 = c_{LBB}|p|_{\mathcal{T},0}\|\boldsymbol{w}\|_1 \geq c_{LBB}|p|_{\mathcal{T},0}\|\widetilde{\boldsymbol{w}}\|_\mathcal{T}, \tag{51}$$

where the function $\widetilde{\boldsymbol{w}} \in \boldsymbol{\mathcal{H}}_\mathcal{T}$ is as defined in Lemma 21. Then we calculate

$$\begin{aligned} B_{\mathcal{D},1}(-\widetilde{\boldsymbol{w}},\widetilde{p}) &= \sum_{K\in\mathcal{T}}\widetilde{p}_K\sum_{s\in\mathcal{V}_K} m_K^s(\widetilde{\nabla}\cdot\Pi_{FV}^{\boldsymbol{u},\boldsymbol{u}}\widetilde{\boldsymbol{w}})_K^s \\ &= \sum_{K\in\mathcal{T}}\sum_{s\in\mathcal{V}_K}\sum_{\sigma\in\mathcal{F}_K\cap\mathcal{F}_s}\widetilde{p}_K\langle\Pi_{FV}^{\boldsymbol{u},\boldsymbol{u}}\widetilde{\boldsymbol{w}} - \Pi_\mathcal{D}\boldsymbol{w}\rangle_{K,s}^\sigma\cdot\boldsymbol{g}_{K,\sigma}^s \\ &\quad + \sum_{K\in\mathcal{T}}\big(\nabla\cdot(\Pi_{L^2}\Pi_\mathcal{D}\boldsymbol{w}-\boldsymbol{w}),p\big)_K + (\nabla\cdot\boldsymbol{w},\widetilde{p}) \\ &\geq \sum_{K\in\mathcal{T}}\sum_{s\in\mathcal{V}_K}\sum_{\sigma\in\mathcal{F}_K\cap\mathcal{F}_s}\widetilde{p}_K\langle\Pi_{FV}^{\boldsymbol{u},\boldsymbol{u}}\widetilde{\boldsymbol{w}} - \Pi_\mathcal{D}\boldsymbol{w}\rangle_{K,s}^\sigma\cdot\boldsymbol{g}_{K,\sigma}^s \\ &\quad - ch|p|_{\mathcal{T},0}\|\boldsymbol{w}\|_1 + c_{LBB}|p|_{\mathcal{T},0}\|\boldsymbol{w}\|_1. \end{aligned} \tag{52}$$

To estimate the remaining summation, we consider jumps across internal edges, exploiting that $\boldsymbol{g}_{K,\sigma}^s = -\boldsymbol{g}_{L,\sigma}^s$ for $\{K,L\} = \mathcal{T}_\sigma$. For simplicity, we introduce $\boldsymbol{\xi}_{K,s}^\sigma = \langle\Pi_{FV}^{\boldsymbol{u},\boldsymbol{u}}\widetilde{\boldsymbol{w}} - \Pi_\mathcal{F}\boldsymbol{w}\rangle_{K,s}^\sigma$, after which

$$\begin{aligned} &\sum_{s\in\mathcal{V}}\sum_{\sigma\in\mathcal{F}_s}\sum_{K\in\mathcal{T}_\sigma}\widetilde{p}_K\langle\Pi_{FV}^{\boldsymbol{u},\boldsymbol{u}}\widetilde{\boldsymbol{w}} - \Pi_\mathcal{F}\boldsymbol{w}\rangle_{K,s}^\sigma\cdot\boldsymbol{g}_{K,\sigma}^s \\ &\qquad = \sum_{s\in\mathcal{V}}\sum_{\sigma\in\mathcal{F}_s}\left(\langle\boldsymbol{\xi}\rangle_s^\sigma + \frac{[[\boldsymbol{\xi}]]_s^\sigma}{2}\right)\left(\langle\widetilde{p}\boldsymbol{g}_{K,\sigma}^s\rangle_s^\sigma + \frac{[[\widetilde{p}\boldsymbol{g}_{K,\sigma}^s]]_s^\sigma}{2}\right) \geq -ch\|\boldsymbol{w}\|_1|p|_\mathcal{T}. \end{aligned} \tag{53}$$

Combining (52)–(53) provides

$$\frac{B_{\mathcal{D},1}(-\widetilde{\boldsymbol{w}},\widetilde{p})}{\|\widetilde{\boldsymbol{w}}\|_\mathcal{T}} \geq (c_{LBB} - ch)|p|_{\mathcal{T},0} - ch|p|_\mathcal{T}. \tag{54}$$

Finally, to treat the constant $\bar{p}$ it is sufficient that there exists a function $\boldsymbol{z} \in \boldsymbol{\mathcal{H}}_{\mathcal{T}}$ such that

$$B_{\mathcal{D},1}(\boldsymbol{z}, 1) \geq c\|\widetilde{\boldsymbol{w}}\|_{\mathcal{T}}. \tag{55}$$

A function such as this exists; thus combining (54) and (55) proves the lemma. ◻

Using Lemma 22, we can now show the stability of the MPSA/MPFA-FV discretization for Biot's equations.

LEMMA 23. *Let Conditions* A, B, *and* C *hold, and let the grid be sufficiently fine such that Lemma* 22 *applies. Furthermore, let the asymmetry of the method be moderate in the sense that* $8\Theta^{\Lambda} < \Theta^{B}$. *Then the discrete system* $\mathfrak{A}_{\mathcal{D}}$ *satisfies the following stability estimate such that for all* $(\boldsymbol{u}, p) \in \boldsymbol{\mathcal{H}}_{\mathcal{T}} \times \mathcal{H}_{\mathcal{T}}$,

$$\begin{aligned}\sup_{(\boldsymbol{v},r)\in\boldsymbol{\mathcal{H}}_{\mathcal{T}}\times\mathcal{H}_{\mathcal{T}}} & \frac{\mathfrak{A}_{\mathcal{D}}(\boldsymbol{u}, p, \boldsymbol{v}, r; \lambda, \rho, \tau)}{\left(\|\boldsymbol{v}\|_{\mathcal{T}}^2 + \tau\|r\|_{\mathcal{T}}^2 + \rho\|r\|_{\mathcal{T},0}^2 + |r|_{\mathcal{T},0}^2\right)^{1/2}} \\ & \geq \Theta^{\mathfrak{A}}\left(\|\boldsymbol{u}\|_{\mathcal{T}}^2 + \tau\|p\|_{\mathcal{T}}^2 + \rho\|p\|_{\mathcal{T},0}^2 + |p|_{\mathcal{T},0}^2\right)^{1/2}.\end{aligned} \tag{56}$$

The constant $\Theta^{\mathfrak{A}}$ *depends on the regularity of the grid and the material parameters but is bounded independent of* $(\rho, \tau, h) \to 0$.

Proof. Recall the nonoptimal stability estimate (49). Furthermore, now let $\boldsymbol{w} \in \boldsymbol{\mathcal{H}}_{\mathcal{D}}$ be the function for which the supremum is achieved in Lemma 22, scaled such that $\|\boldsymbol{w}\|_{\mathcal{T}} = |p|_{\mathcal{T},0}$. Then, for $(\boldsymbol{v}, r) = (\boldsymbol{u} - \delta\boldsymbol{w}, -p)$,

$$\begin{aligned}\mathfrak{A}_{\mathcal{D}}(\boldsymbol{u}, p, \boldsymbol{v}, r) &= \mathfrak{A}_{\mathcal{D}}(\boldsymbol{u}, p, \boldsymbol{u}, -p) + \delta\mathfrak{A}_{\mathcal{D}}(-\boldsymbol{w}, 0, \boldsymbol{u}, p) \\ &\geq \Theta^{A}\|\boldsymbol{u}\|_{\mathcal{T}}^2 + \tau\Theta^{C}\|p\|_{\mathcal{T}}^2 + h^2\Theta^{\Delta}|p|_{\mathcal{T}}^2 + \rho\|p\|_{\mathcal{T},0}^2 + \delta\Theta^{B}|p|_{\mathcal{T},0}^2 \\ &\quad - (\Theta^{\Lambda} + \delta\Theta^{A})\|\boldsymbol{u}\|_{\mathcal{T}}|p|_{\mathcal{T},0} - \delta h\theta^{B}|p|_{\mathcal{T},0}|p|_{\mathcal{T}}.\end{aligned} \tag{57}$$

This inequality holds subject to the negative terms being controlled by the positive terms, which implies the following conditions:

$$4(\Theta^{\Lambda} + \delta\Theta^{A})^2 \leq \gamma_1\Theta^{A}\delta\Theta^{B} \quad \text{and} \quad 4(\delta h\theta^{B})^2 \leq \gamma_2 h^2\Theta^{\Delta}\delta\Theta^{B}. \tag{58}$$

For the two conditions, we find that by differentiating the left-hand inequality of (58) to obtain the optimal δ and determining γ_2 from the right-hand inequality of (58) implies the two equalities

$$\delta = \frac{\gamma_1\Theta^{B} - 8\Theta^{\Lambda}}{8\Theta^{A}} \quad \text{and} \quad \gamma_2 = \frac{4\delta(\theta^{B})^2}{\Theta^{\Delta}\Theta^{B}}. \tag{59}$$

Recall that $\gamma_2 = 1 - \gamma_1$ such that we can simplify equations (59) to obtain

$$\gamma_1 = \frac{2\Theta^{A}\Theta^{\Delta}\Theta^{B}(\theta^{B})^{-2} + 8\Theta^{\Lambda}}{2\Theta^{A}\Theta^{\Delta}\Theta^{B}(\theta^{B})^{-2} + \Theta^{B}}. \tag{60}$$

We see that (60) implies that $\gamma_1 > 0$, while for $\gamma_1 < 1$ it must also hold that

$$8\Theta^{\Lambda} < \Theta^{B}, \tag{61}$$

while also by substituting (60) into either of equations (59) and the left-hand inequality of (58) we obtain

$$8\Theta^{\Lambda} \leq \gamma_1\Theta^{B}. \tag{62}$$

However, substituting (60) into (58), we note that (62) always holds whenever (61) holds, which thus remains the sole condition in the proof. Subject to this condition we then have the inequality

$$\mathfrak{A}_{\mathcal{D}}(\boldsymbol{u}, p, \boldsymbol{v}, r) \geq C_1\big(\|\boldsymbol{u}\|^2_{\mathcal{T}} + \tau\|p\|^2_{\mathcal{T}} + \rho\|p\|^2_{\mathcal{T},0} + |p|^2_{\mathcal{T},0}\big).$$

Since we have explicitly retained all dependencies, it is clear that the stability constant C_1 depends on all constants Θ in (57), but is independent of ρ, τ, and h, as asserted. Finally, the lemma follows since

$$\begin{aligned}(63)\quad \|\boldsymbol{u} - \delta\boldsymbol{w}\|^2_{\mathcal{T}} + \tau\|p\|^2_{\mathcal{T}} + \rho\|p\|^2_{\mathcal{T},0} + |p|^2_{\mathcal{T},0} &\\ \leq \|\boldsymbol{u}\|^2_{\mathcal{T}} + \tau\|p\|^2_{\mathcal{T}} + \rho\|p\|^2_{\mathcal{T},0} + [1+\delta^2]|p|^2_{\mathcal{T},0}&\\ \leq C_2(\|\boldsymbol{u}\|^2_{\mathcal{T}} + \tau\|p\|^2_{\mathcal{T}} + \rho\|p\|^2_{\mathcal{T},0} + |p|^2_{\mathcal{T},0}).&\end{aligned}$$

Equation (59) shows that δ is bounded from above independently of ρ, τ, and h; thus the constant C_2 is also bounded independent of all coefficients stated in the lemma, and finally we obtain the lemma with the constant defined as $\Theta^{\mathfrak{A}} = C_1/\sqrt{C_2}$. ∎

COROLLARY 24. *The MPFA/MPSA-FV discretization is robust in the sense of Definition* 1*, and all eigenvalues of the system* $\mathfrak{A}_{\mathcal{D}}(\boldsymbol{u}, p, \boldsymbol{v}, r; \rho, \tau)$ *are bounded away from zero.*

Remark 25. Lemma 23 has a requirement on the grid, which states that the asymmetry of the coupling terms induced by $\Lambda_{\mathcal{D}}$ must be sufficiently small, relative to (essentially) the inf-sup constant. Since Θ^{Λ} can be locally calculated based on the constants in Definition 17, this condition is locally estimated at the time of discretization assembly for general grids and can be verified a priori for regular grids. We will return to this condition in section 6.3. Furthermore, following Comment 8, we note that for the symmetric discretization on simplex grids, local conditions (Conditions A and B) are automatically satisfied, and $\Theta^{\Lambda} = 0$.

5.4. Compactness results. The stability established in Lemma 23 will suffice to show convergence after generalizing a few standard results for the uncoupled discretizations.

DEFINITION 26. *We consider the following continuous extensions of the cell-average FV gradients for discrete functions* $\boldsymbol{u} \in \boldsymbol{\mathcal{H}}_{\mathcal{D}}$ *(and equivalently for scalar functions* $p \in \mathcal{H}_{\mathcal{D}}$*):*

$$(64)\qquad \nabla_{\mathcal{D}}\boldsymbol{u}(\boldsymbol{x}) = (\widetilde{\nabla}\boldsymbol{u})_K \quad \text{for } K \in \mathcal{T},\ \text{where } \boldsymbol{x} \in K.$$

Furthermore, we consider the continuous extension of the consistent gradient

$$(65)\qquad \overline{\nabla}_{\mathcal{D}}\boldsymbol{u}(\boldsymbol{x}) = (\overline{\nabla}\boldsymbol{u})^s_K \quad \text{for } K \in \mathcal{T},\ s \in \mathcal{T},\ \text{where } \boldsymbol{x} \in K_s.$$

LEMMA 27. *Fix* $\tau > 0$*, and let* $\mathcal{D}_n$ *be a family of regular discretization triplets (in the sense that mesh parameters remain bounded) such that* $h_n \to 0$ *as* $n \to \infty$*. Furthermore, let the conditions of Lemma 23 hold. Then, for all* n*, the solutions* $(\boldsymbol{u}_n, p_n)$ *of* (37)–(38) *exist and are unique, there exists* $(\widetilde{\boldsymbol{u}}, \widetilde{p}) \in (H^1(\Omega))^d \times H^1(\Omega)$*, and up to a subsequence (still denoted by* n*)* $\Pi_{\mathcal{T}}\boldsymbol{u}_n \to \widetilde{\boldsymbol{u}}$ *and* $\Pi_{\mathcal{T}}p_n \to \widetilde{p}$ *converge in* $(L^q(\Omega))^d \times L^q(\Omega)$ *for* $q \in [1, 2d/(d-2+\epsilon))$ *as* $h_n \to 0$*. Finally, the cell-average FV gradients* $\nabla_{\mathcal{D}}\boldsymbol{u}_n$ *and* $\nabla_{\mathcal{D}}p_n$ *converge weakly to* $\nabla\widetilde{\boldsymbol{u}}$ *in* $(L^2(\Omega))^{d^2}$ *and* $\nabla\widetilde{p}$ *in* $(L^2(\Omega))^d$*, respectively.*

Proof. The proof follows from the stability of the scheme, Lemma 23, and the compactness arguments detailed in [16, 6]. ☐

LEMMA 28. *Consider the same case as in Lemma* 27. *Then the consistent gradients* $\overline{\nabla}_{\mathcal{D}}\boldsymbol{u}_n$ *and* $\overline{\nabla}_{\mathcal{D}}p_n$ *converge strongly to* $\nabla\widetilde{\boldsymbol{u}}$ *in* $(L^2(\Omega))^{d^2}$ *and* $\nabla\widetilde{p}$ *in* $(L^2(\Omega))^d$, *respectively.*

Proof. The proof is stated in [3] (scalar case) and [29] (vector case). ☐

Remark 29. In the limiting case $\tau = 0$, the regularity of pressure is reduced such that $\widetilde{p} \in L^2(\Omega)$. Consequently, we do not discuss convergence of $\nabla_{\mathcal{D}}p_n$ and $\overline{\nabla}_{\mathcal{D}}p_n$ in this case.

5.5. Convergence. We summarize the results of this section in the main convergence result for the method.

THEOREM 30. *Let* $\mathcal{D}_n$ *be a family of regular discretization triplets (in the sense that mesh parameters remain bounded) such that* $h_n \to 0$ *as* $n \to \infty$, *let Conditions* A, B, *and* C *hold with constants independent of* n, *and let* $8\Theta^\Lambda < \Theta^B$. *Then for* $\tau > 0$ *the limit* $(\widetilde{\boldsymbol{u}}, \widetilde{p}) \in (H^1(\Omega))^d \times H^1(\Omega)$ *of the discrete mixed variational problem* (37)–(38), *and consequently the MPSA/MPFA discretizations for the Biot equations, is the unique weak solution of the Biot problem* (1).

Proof. Lemmas 27 and 28 establish that the limit $(\widetilde{\boldsymbol{u}}, \widetilde{p}) \in (H^1(\Omega))^d \times H^1(\Omega)$ exists and establish the appropriate notion of convergence of the discrete gradients. It remains to show that the solution pair $(\widetilde{\boldsymbol{u}}, \widetilde{p})$ is consistent with the weak form of problem (1). Uniqueness then follows from the uniqueness of weak solutions to (1). We show consistency by projecting continuous functions into the discrete spaces and note that we suppress the dependence of $\Pi_{\mathcal{T}}$ and Π_{FV} on n.

For all $\boldsymbol{u}, \boldsymbol{v} \in (C^\infty(\Omega))^d$,

$$\lim_{n\to\infty} a_{\mathcal{D}_n}(\Pi_{FV}^{\boldsymbol{u},\boldsymbol{u}}\Pi_{\mathcal{T}}\boldsymbol{u}, \boldsymbol{v}) = \int_\Omega (\mathbb{C} : \nabla\boldsymbol{u}) : \nabla\boldsymbol{v}\, d\boldsymbol{x}. \tag{66}$$

For all $\boldsymbol{u} \in (C^\infty(\Omega))^d$ and $r \in C^\infty(\Omega)$.

$$\lim_{n\to\infty} b_{\mathcal{D}_n,1}(\Pi_{FV}^{\boldsymbol{u},\boldsymbol{u}}\Pi_{\mathcal{T}}\boldsymbol{u}, r) = -\int_\Omega r\nabla\cdot\boldsymbol{u}\, d\boldsymbol{x}. \tag{67}$$

For all $\boldsymbol{v} \in (C^\infty(\Omega))^d$ and $p \in C^\infty(\Omega)$,

$$\lim_{n\to\infty} a_{\mathcal{D}_n}(\Pi_{FV}^{\boldsymbol{u},p}\Pi_{\mathcal{T}}p, \boldsymbol{v}) = -\int_\Omega p\nabla\cdot\boldsymbol{v}\, d\boldsymbol{x}. \tag{68}$$

For all $p, r \in C^\infty(\Omega)$,

$$\lim_{n\to\infty} c_{\mathcal{D}_n}(\Pi_{FV}^{p}\Pi_{\mathcal{T}}p, r) = -\int_\Omega (k\nabla p)\cdot\nabla r\, d\boldsymbol{x}. \tag{69}$$

For all $p, r \in C^\infty(\Omega)$,

$$\lim_{n\to\infty} b_{\mathcal{D}_n,1}(\Pi_{FV}^{\boldsymbol{u},p}\Pi_{\mathcal{T}}p, r) = 0. \tag{70}$$

For all $\boldsymbol{v} \in (C^\infty(\Omega))^d$,

$$\lim_{n\to\infty} \int_\Omega \boldsymbol{f}_{\boldsymbol{u}}\cdot\Pi_{\mathcal{T}}\boldsymbol{v}\, d\boldsymbol{x} = \int_\Omega \boldsymbol{f}_{\boldsymbol{u}}\cdot\boldsymbol{v}\, d\boldsymbol{x}. \tag{71}$$

For all $r \in (C^\infty(\Omega))^d$,

$$\lim_{n\to\infty} \int_\Omega f_p \cdot \Pi_{\mathcal{T}} r \, d\boldsymbol{x} = \int_\Omega f_p \cdot r \, d\boldsymbol{x}. \tag{72}$$

Since the right-hand sides of (65)–(72) form the weak form of equations (1), and since C^∞ is dense in H^1, it follows that the limit $(\widetilde{\boldsymbol{u}}, \widetilde{p})$ is a weak solution to (1). ☐

5.6. Fully time-discrete scheme. From (1) and (36), we note that the time-iterative scheme for the solution $(\boldsymbol{u}_{\mathcal{T}}^j, p_{\mathcal{T}}^j)$ at time-step j, written in terms of the solution at time-step $j-1$, is

$$\mathfrak{A}_{\mathcal{D}}(\boldsymbol{u}_{\mathcal{T}}^j, p_{\mathcal{T}}^j, \boldsymbol{v}, r; \rho, \tau) = \mathfrak{A}_{\mathcal{D}}(\boldsymbol{u}_{\mathcal{T}}^{j-1}, p_{\mathcal{T}}^{j-1}, \boldsymbol{v}, r; \rho, 0) + \mathfrak{B}(\boldsymbol{0}, r) \quad \text{for all } (\boldsymbol{v}, r) \in \boldsymbol{\mathcal{H}}_{\mathcal{T}} \times \mathcal{H}_{\mathcal{T}}. \tag{73}$$

In terms of linear systems, this is equivalent to the matrix system

$$\mathfrak{a}_{\mathcal{D}}(\rho,\tau) \cdot \begin{pmatrix} \boldsymbol{u}_{\mathcal{T}}^j \\ p_{\mathcal{T}}^j \end{pmatrix} = \mathfrak{a}_{\mathcal{D}}(\rho,0) \cdot \begin{pmatrix} \boldsymbol{u}_{\mathcal{T}}^{j-1} \\ p_{\mathcal{T}}^{j-1} \end{pmatrix} + \mathfrak{b} \cdot \begin{pmatrix} \boldsymbol{0} \\ r \end{pmatrix},$$

where the matrix $\mathfrak{a}_{\mathcal{D}}(\rho,\tau)$ corresponds to the values of $\mathfrak{A}_{\mathcal{D}}(\boldsymbol{u}, p, \boldsymbol{v}, r; \rho, \tau)$ with $(\boldsymbol{u}, p, \boldsymbol{v}, r)$ chosen as the canonical basis. Define the error as

$$e_{\mathcal{T}}^j = \begin{pmatrix} \boldsymbol{u}_{\mathcal{T}}^j - \boldsymbol{u}^j \\ p_{\mathcal{T}}^j - p^j \end{pmatrix}.$$

Then, from Lemma 23 and the Poincaré inequality, it follows that for $\tau > 0$ we obtain a stable time-discretization since

$$\sup_{e_{\mathcal{T}}^{j-1}} \frac{\|e_{\mathcal{T}}^j\|_0}{\|e_{\mathcal{T}}^{j-1}\|_0} = \sup_{e_{\mathcal{T}}^{j-1}} \frac{\|\mathfrak{a}_{\mathcal{D}}^{-1}(\rho,\tau) \cdot \mathfrak{a}_{\mathcal{D}}(\rho,0) \cdot e_{\mathcal{T}}^{j-1}\|_0}{\|e_{\mathcal{T}}^{j-1}\|_0} = \|\mathfrak{a}_{\mathcal{D}}^{-1}(\rho,\tau) \cdot \mathfrak{a}_{\mathcal{D}}(\rho,0)\| < 1.$$

Thus, the time-discrete problem is also stable, independent of time-step, and convergent due to the consistency of the first-order truncation error in backward Euler (implicit) discretization (see, e.g., [23]).

6. Numerical validation.

Herein, we restrict our attention towards verifying the claims that the method is (a) robust according to Definition 1, (b) stable as stated in Lemma 23, and (c) convergent as stated in Theorem 30. We refer the reader to the works on related methods to give a general impression of this class of methods for complex grids [27, 22] and solutions with low regularity [13]. Together, the above references give numerical evidence of the suitability of the individual discretizations $A_{\mathcal{D}}$ and $C_{\mathcal{D}}$.

6.1. Problem formulation. As a test problem, we consider the unit square in two spatial dimensions. We choose as an analytical solution the function

$$\boldsymbol{u}(x_1, x_2) = \begin{pmatrix} x_1(1-x_1)\sin(2\pi x_2) \\ \sin(2\pi x_1)\sin(2\pi x_2) \end{pmatrix} \tag{74}$$

and $p = \boldsymbol{u} \cdot \boldsymbol{e}_1$. These functions satisfy zero Dirichlet boundary conditions, and the problem is thus driven by internal source-sink terms (for the flow equation) and body-forces (for the momentum equation). We calculate these right-hand-side functions analytically according to equations (1), using unit permeability and Lamé parameters, in the sense that we consider an isotropic material with the properties

$$\mathbb{C} : \nabla \boldsymbol{u} = \nabla \boldsymbol{u} + \nabla \boldsymbol{u}^T + (\nabla \cdot u)\boldsymbol{I}.$$

This implies a Poisson ratio of 0.25, which is within the typical range of natural materials.

We consider three types of grids. Type A is a standard Cartesian grid, type B is a simplex grid obtained by bisecting the Cartesian grid, and type C is a dual-simplex grid obtained by taking the dual grid to the corresponding type B grid. Type C grids are related to PEBI grids and are representative of unstructured grids. For grid types A and C we use the general method with second-order quadrature for evaluating the jump terms, while for grid type B we use the simplified symmetric discretization as discussed in Comment 8.

For the grid refinement, we consider seven refinement levels, where the grid vertexes at each refinement level are perturbed randomly by a factor between $\pm h/2$. Thus we consider so-called rough grids [21], without the milder assumption that the grid asymptotically is only h^2 perturbed, the latter of which is typical for methods derived from mixed finite elements using numerical quadrature (see, e.g., [38]). These rough grids are representative of grid regularity as experienced in geological subsurface applications.

The grids are illustrated in Figure 1, together with the structure of the analytical solution (74). For all figures, the third refinement level is shown.

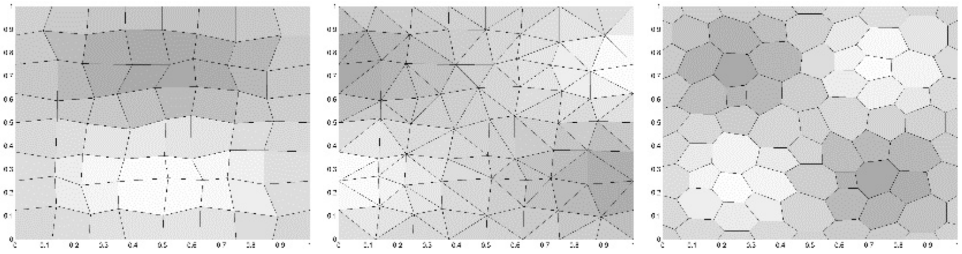

FIG. 1. *From left to right the figures illustrate grid types A (quadrilaterals), B (triangles), and C (unstructured grids). Furthermore, in greyscale, the figures indicate the structure of the analytical solution from* (74)*: the first component of the displacement vector (which is equal to pressure), the first component of the pressure gradient, and the second component of the displacement vector, respectively.*

6.2. Convergence results. In the reported results, we consider errors using the following L^2-type metrics:

$$\epsilon_{\boldsymbol{u}} = \frac{\|\boldsymbol{u}_{\mathcal{T}} - \Pi_{\mathcal{T}} \boldsymbol{u}\|_{\mathcal{T},0}}{\|\Pi_{\mathcal{T}} \boldsymbol{u}\|_{\mathcal{T},0}}, \tag{75}$$

$$\epsilon_p = \frac{\|p_{\mathcal{T}} - \Pi_{\mathcal{T}} p\|_{\mathcal{T},0}}{\|\Pi_{\mathcal{T}} p\|_{\mathcal{T},0}}, \tag{76}$$

$$\epsilon_{p,|} = \frac{|p_{\mathcal{T}} - \Pi_{\mathcal{T}} p|_{\mathcal{T},0}}{\|\Pi_{\mathcal{T}} p\|_{\mathcal{T},0}}, \tag{77}$$

$$\epsilon_{\boldsymbol{\pi}} = \frac{\sum_{\sigma \in \mathcal{F}} m_\sigma^2 [\boldsymbol{T}_K^\sigma - \boldsymbol{\pi}(\boldsymbol{x}_\sigma) \cdot \boldsymbol{n}_{K,\sigma}]^2}{\sum_{\sigma \in \mathcal{F}} m_\sigma^2 [\boldsymbol{\pi}(\boldsymbol{x}_\sigma) \cdot \boldsymbol{n}_{K,\sigma}]^2}, \tag{78}$$

$$\epsilon_q = \frac{\sum_{\sigma\in\mathcal{F}} m_\sigma^2 [q_K^\sigma - \boldsymbol{q}(\boldsymbol{x}_\sigma)\cdot \boldsymbol{n}_{K,\sigma}]^2}{\sum_{\sigma\in\mathcal{F}} m_\sigma^2 [\boldsymbol{q}(\boldsymbol{x}_\sigma)\cdot \boldsymbol{n}_{K,\sigma}]^2}. \tag{79}$$

Here the discrete flux and traction are defined in (17) and (20), utilizing that due to (18) and (21) we can (up to the sign) evaluate the expression for either $K \in \mathcal{T}_\sigma$. In order to show stability according to Definition 1 and verify Lemma 23, we combine the above errors to the *stable error*

$$\epsilon_\Sigma = \epsilon_{\boldsymbol{u}} + \epsilon_{\boldsymbol{\pi}} + (\tau+\rho)\epsilon_p + \tau\epsilon_q + \epsilon_{p,|}. \tag{80}$$

In order to illustrate the numerical convergence rate of the primary variables, we give the *primary error* associated with the primary variables displacement and pressure as

$$\epsilon_{\boldsymbol{u},p} = \epsilon_{\boldsymbol{u}} + \tau\epsilon_p. \tag{81}$$

Note that the primary error does not provide control on pressure or flux in the limit of $\tau \to 0$; we include it in order to highlight better spatial convergence rates.

For the convergence study, we consider all combinations of $(\rho,\tau) \in [1, 10^{-2}, 10^{-4}, 10^{-6}]^2$. All computations are performed using MATLAB on a standard laptop. The full study contains $3\times 7\times 5\times 5 = 525$ computations, the results of which are summarized in the tables below.

In Tables 1 and 2 we give the results for the stable error ϵ_Σ on rough grids. As expected, the discretization is robust, and we obtain (better than) first-order convergence independent of small parameters. Moreover, the error constant is bounded as expected from Lemma 23.

In Tables 3 and 4 we give the results for the primary error $\epsilon_{\boldsymbol{u},p}$ on rough grids. For these results we observe second-order convergence, again with constants independent of the small parameters.

We summarize the results of Tables 1 through 4 heuristically as follows.

Statement 31. For h-perturbed grids the MPFA/MPSA-FV method displays a numerical convergence following

$$h^{-1}\epsilon_\Sigma + h^{-2}\epsilon_{\boldsymbol{u},p} < C, \tag{82}$$

where the constant C does not depend on τ or ρ.

6.3. Local conditions.

For all grids in the test suite, we considered the local conditions (Conditions A, B, and C), as well as the asymmetry condition $8\Theta^\Lambda < \Theta^B$ arising in Lemma 23. As noted in Remark 25, all but Condition C are immediate on simplex grids. Furthermore, for all grids of types A and C, the local conditions were satisfied, testifying to the statement that these conditions are not restrictive in practice. We emphasize the fact that the local conditions are independent of the parameters ρ and τ.

However, this is not to imply that there do not exist grids where the local conditions are not satisfied. Indeed, expressions similar to Condition B, which pertains to the local coercivity of the discretization of the flow equations, can be violated on severely skewed parallelograms, as discussed previously [21], which can be linked to a loss of monotonicity of the scheme [30].

7. Conclusion.

We provide a new FV method for the Biot equations. The method is distinguished by the following properties:

Table 1

Asymptotic convergence rate of stable error ϵ_Σ for grids of types A, B, and C.

ϵ_Σ	$\tau = 1$			$\tau = 10^{-1}$			$\tau = 10^{-2}$			$\tau = 10^{-4}$			$\tau = 10^{-6}$		
Grid	A	B	C	A	B	C	A	B	C	A	B	C	A	B	C
$\rho = 1$	1.36	1.36	1.27	1.45	1.51	1.48	1.63	1.68	1.75	2.01	1.90	1.97	1.09	1.14	1.16
$\rho = 10^{-1}$	1.33	1.32	1.23	1.40	1.46	1.41	1.64	1.66	1.73	2.16	1.89	2.02	1.17	1.25	1.25
$\rho = 10^{-2}$	1.32	1.32	1.23	1.40	1.45	1.40	1.64	1.66	1.73	2.16	1.88	2.00	1.20	1.29	1.28
$\rho = 10^{-4}$	1.32	1.32	1.23	1.40	1.45	1.40	1.64	1.66	1.73	2.16	1.88	2.00	1.20	1.29	1.29
$\rho = 10^{-6}$	1.32	1.32	1.23	1.40	1.45	1.40	1.64	1.66	1.73	2.16	1.88	2.00	1.20	1.29	1.29

Table 2

Asymptotic stable error ϵ_Σ for grids of types A, B, and C.

ϵ_Σ	$\tau = 1$			$\tau = 10^{-1}$			$\tau = 10^{-2}$			$\tau = 10^{-4}$			$\tau = 10^{-6}$		
Grid	A	B	C	A	B	C	A	B	C	A	B	C	A	B	C
$\rho = 1$	.006	.005	.006	.006	.006	.005	.009	.012	.010	.029	.034	.022	.092	.121	.062
$\rho = 10^{-1}$	.006	.005	.006	.005	.005	.005	.009	.012	.010	.026	.040	.026	.133	.171	.088
$\rho = 10^{-2}$	.006	.005	.006	.005	.005	.004	.009	.012	.010	.026	.043	.029	.146	.187	.096
$\rho = 10^{-4}$	.006	.005	.006	.005	.005	.004	.009	.012	.010	.027	.044	.029	.148	.189	.098
$\rho = 10^{-6}$	.006	.005	.006	.005	.005	.004	.009	.012	.010	.027	.044	.029	.148	.189	.098

Table 3

Asymptotic convergence rate of primary error $\epsilon_{\boldsymbol{u},p}$ for grids of types A, B, and C.

$\epsilon_{\boldsymbol{u},p}$	$\tau = 1$			$\tau = 10^{-1}$			$\tau = 10^{-2}$			$\tau = 10^{-4}$			$\tau = 10^{-6}$		
Grid	A	B	C	A	B	C	A	B	C	A	B	C	A	B	C
$\rho = 1$	2.00	1.97	1.99	1.98	1.93	1.98	1.99	1.94	1.98	1.99	1.95	1.99	1.99	1.95	1.98
$\rho = 10^{-1}$	2.00	1.97	1.99	1.98	1.92	1.98	1.99	1.93	1.97	1.99	1.94	1.98	1.98	1.94	1.98
$\rho = 10^{-2}$	2.00	1.97	1.99	1.98	1.92	1.98	1.99	1.93	1.97	1.98	1.93	1.97	1.98	1.94	1.98
$\rho = 10^{-4}$	2.00	1.97	1.99	1.98	1.92	1.98	1.99	1.93	1.97	1.98	1.93	1.97	1.98	1.94	1.98
$\rho = 10^{-6}$	2.00	1.97	1.99	1.98	1.92	1.98	1.99	1.93	1.97	1.98	1.93	1.97	1.98	1.94	1.98

Table 4

Asymptotic primary error $\epsilon_{\boldsymbol{u},p}$ for grids of types A, B, and C. All numbers are scaled by 10^{-3}.

$\epsilon_{\boldsymbol{u},p}$	$\tau = 1$			$\tau = 10^{-1}$			$\tau = 10^{-2}$			$\tau = 10^{-4}$			$\tau = 10^{-6}$		
Grid	A	B	C	A	B	C	A	B	C	A	B	C	A	B	C
$\rho = 1$	1.14	0.84	0.69	0.91	0.72	0.51	0.87	0.67	0.48	0.85	0.64	0.47	0.85	0.64	0.47
$\rho = 10^{-1}$	1.14	0.84	0.69	0.92	0.74	0.52	0.89	0.71	0.52	0.88	0.71	0.58	0.88	0.71	0.58
$\rho = 10^{-2}$	1.14	0.84	0.69	0.92	0.74	0.52	0.89	0.72	0.53	0.90	0.75	0.63	0.90	0.74	0.63
$\rho = 10^{-4}$	1.14	0.84	0.69	0.92	0.74	0.52	0.89	0.72	0.53	0.90	0.75	0.64	0.90	0.75	0.64
$\rho = 10^{-6}$	1.14	0.84	0.69	0.92	0.74	0.52	0.89	0.72	0.53	0.90	0.75	0.64	0.90	0.75	0.64

- The variables are cell-centered for both displacement and pressure, allowing for sparse linear systems and efficient data structure. This is in contrast to the industry-standard discretizations using staggered grids.
- The discretization is valid for general grids in two and three dimensions, with only local constraints on grid and parameters. Numerical examples indicate that these constraints are mild.
- The discretization is naturally stable in the sense of Definition 1.

For the proposed discretization, we provide stability analysis and convergence proof utilizing the framework of hybrid FV methods. The analysis exploits techniques from VMS methods and stabilized mixed finite element methods and does not rely on assumptions of asymptotic grid regularity.

Finally, we provide numerical evidence justifying the stability analysis. The numerical examples indicate that for rough grids (h-perturbed) we have a general second-order convergence of the scheme in terms of primary variables (displacement and pressure). The convergence of secondary variables (traction and normal fluxes) is in general first order. In the limit where $\tau \to 0$, the convergence rate of pressure is reduced to first order, while the convergence of fluxes is lost. This is consistent with the expected regularity of the solution.

REFERENCES

[1] I. Aavatsmark, *An introduction to the multipoint flux approximations for quadrilateral grids*, Comput. Geosci., 6 (2002), pp. 405–432, doi:10.1023/A:1021291114475.

[2] I. Aavatsmark, T. Barkve, Ø. Bøe, and T. Mannseth, *Discretization on non-orthogonal, quadrilateral grids for inhomogeneous, anisotropic media*, J. Comput. Phys., 127 (1996), pp. 2–14, doi:10.1006/jcph.1996.0154.

[3] L. Agelas, C. Guichard, and R. Masson, *Convergence of finite volume MPFA O type schemes for heterogeneous anisotropic diffusion problems on general meshes*, Int. J. Finite Vol., 7 (2010), no. 2.

[4] L. Agelas and R. Masson, *Convergence of finite volume MPFA O type schemes for heterogeneous anisotropic diffusion problems on general meshes*, C. R. Math. Acad. Sci. Paris, 246 (2008), pp. 1007–1012, doi:10.1016/j.crma.2008.07.015.

[5] T. Arbogast, *Analysis of a two-scale, locally conservative subgrid upscaling for elliptic problems*, SIAM J. Numer. Anal., 42 (2004), pp. 576–598, doi:10.1137/S0036142902406636.

[6] D. Arnold and R. Winther, *Mixed finite elements for elasticity*, Numer. Math., 92 (2002), pp. 401–419, doi:10.1007/s002110100348.

[7] I. Babuska, *Error bounds for finite element method*, Numer. Math., 16 (1971), pp. 322–333, doi:10.1007/BF02165003.

[8] S. Badia, A. Quaini, and A. Quarteroni, *Coupling Biot and Navier-Stokes equations for modelling fluid-poroelastic media interaction*, J. Comput. Phys., 228 (2009), pp. 7986–8014, doi:10.1016/j.jcp.2009.07.019.

[9] M. A. Biot, *General theory of three dimensional consolidation*, J. Appl. Phys., 12 (1941), pp. 155–164, doi:10.1063/1.1712886.

[10] F. Brezzi, *On the existence, uniqueness and approximation of saddle-point problems arising from Lagrange multipliers*, Rev. Française Automat. Informat. Recherche Opérationnelle Sér. Rouge, 8 (1974), pp. 129–151.

[11] F. Brezzi and M. Fortin, *Mixed and Hybrid Finite Element Methods*, Springer Ser. Comput. Math. 15, Springer-Verlag, New York, 1991.

[12] F. Brezzi and J. Pitkäranta, *On the stabilization of finite element approximations of the Stokes problem*, in Efficient Solutions of Elliptic Systems, Notes Numer. Fluid Mech. 10, Friedrich Vieweg, Braunschweig, 1984, pp. 11–19.

[13] G. T. Eigestad and R. Klausen, *On the convergence of the multi-point flux approximation O-method: Numerical experiments for discontinuous permeability*, Numer. Methods Partial Differential Equations, 21 (2005), pp. 1079–1098, doi:10.1002/num.20079.

[14] R. Eymard, T. Gallouët, and R. Herbin, *Finite volume methods*, in Handbook of Numerical Analysis, Vol. VII, Elsevier, Amsterdam, 2006, pp. 713–1020, doi:10.1016/S1570-8659(00)07005-8.

[15] L. P. Franca and R. Stenberg, *Error analysis of some Galerkin least squares methods for the elasticity equations*, SIAM J. Numer. Anal., 28 (1991), pp. 1680–1697, doi:10.1137/0728084.

[16] F. J. Gaspar, F. J. Lisbona, and C. W. Oosterlee, *A stabilized difference scheme for deformable porous media and its numerical resolution by multigrid methods*, Comput. Vis. Sci., 11 (2008), pp. 67–76, doi:10.1007/s00791-007-0061-1.

[17] F. J. Gaspar, F. J. Lisbona, and P. N. Vabishchevich, *Staggered grid discretizations for the quasi-static Biot's consolidation problem*, Appl. Numer. Math., 56 (2006), pp. 888–898, doi:10.1016/j.apnum.2005.07.002.

[18] J. B. Haga, H. Osnes, and H. P. Langtangen, *On the causes of pressure oscillations in*

low-permeable and low-compressible porous media, Internat. J. Numer. Anal. Methods Geomech., 36 (2012), pp. 1507–1522, doi:10.1002/nag.1062.

[19] T. J. R. Hughes, G. R. Feijoo, L. Mazzei, and J. B. Quincy, *The variational multiscale method—a paradigm for computational mechanics*, Comput. Methods Appl. Mech. Engrg., 166 (1998), pp. 3–24, doi:10.1016/S0045-7825(98)00079-6.

[20] H. Jasak and H. G. Weller, *Application of the finite volume method and unstructured meshes to linear elasticity*, Internat. J. Numer. Methods Engrg., 48 (2000), pp. 267–287, doi:10.1002/(SICI)1097-0207(20000520)48:2⟨267::AID-NME884⟩3.0.CO;2-Q.

[21] R. Klausen and R. Winther, *Robust convergence of multi point flux approximation on rough grids*, Numer. Math., 104 (2006), pp. 317–337, doi:10.1007/s00211-006-0023-4.

[22] R. A. Klausen and A. F. Stephansen, *Convergence of multi-point flux approximation on general grids and media*, Int. J. Numer. Anal. Model., 9 (2012), pp. 584–606.

[23] R. Leveque, *Finite Volume Methods for Hyperbolic Problems*, Cambridge University Press, Cambridge, UK, 2002, doi:10.1017/CBO9780511791253.

[24] R. W. Lewis and B. A. Schrefler, *The Finite Element Method in the Static and Dynamic Deformation and Consolidation of Porous Media*, John Wiley and Sons, Chichester, UK, 1998, doi:10.1002/(SICI)1099-1484(200001)5:1⟨85::AID-CFM94⟩3.0.CO;2-8.

[25] J. C. Nagtegaal, D. M. Parks, and J. R. Rice, *On numerically accurate finite element solutions in the fully plastic range*, Comput. Methods Appl. Mech. Engrg., 4 (1974), pp. 153–177, doi:10.1016/0045-7825(74)90032-2.

[26] J. M. Nordbotten, *Adaptive variational multiscale methods for multiphase flow in porous media*, Multiscale Model. Simul., 7 (2009), pp. 1455–1473, doi:10.1137/080724745.

[27] J. M. Nordbotten, *Cell-centered finite volume discretizations for deformable porous media*, Internat. J. Numer. Methods Engrg., 100 (2014), pp. 399–418, doi:10.1002/nme.4734.

[28] J. M. Nordbotten, *Finite volume hydro-mechanical simulation of porous media*, Water Resour. Res., 50 (2014), pp. 4379–4394, doi:10.1002/2013WR015179.

[29] J. M. Nordbotten, *Convergence of a cell-centered finite volume discretization for linear elasticity*, SIAM J. Numer. Anal., 53 (2015), pp. 2605–2625, doi:10.1137/140972792.

[30] J. M. Nordbotten, I. Aavatsmark, and G. Eigestad, *Monotonicity of control volume methods*, Numer. Math., 106 (2007), pp. 255–288, doi:10.1007/s00211-006-0060-z.

[31] J. M. Nordbotten and M. A. Celia, *Geological Storage of CO_2: Modeling Approaches for Large-Scale Simulation*, Wiley, New York, 2011, ISBN: 978-1-118-13707-9.

[32] T. F. Russell and M. F. Wheeler, *Finite element and finite difference methods for continuous flows in porous media*, in Mathematics of Reservoir Simulation, R. E. Ewing, ed., SIAM, Philadelphia, 1983, pp. 35–106, doi:10.1137/1.9781611971071.ch2.

[33] J. Rutquist, D. W. Vasco, and L. Myer, *Coupled reservoir-geomechanical analysis of CO_2 injection and ground deformations at In Salah*, Int. J. Greenh. Gas Control, 4 (2010), pp. 225–230, doi:10.1016/j.ijggc.2009.10.017.

[34] R. Temam and A. Miramville, *Mathematical Modeling in Continuum Mechanics*, Cambridge University Press, Cambridge, UK, 2000, doi:10.1017/CBO9780511755422.

[35] J. W. Tester, *The Future of Geothermal Energy*, Report INL/EXT-06-1174, MIT, Cambridge, MA, 2006.

[36] M. Wheeler, G. Xue, and I. Yotov, *A multipoint flux mixed finite element method on distorted quadrilaterals and hexahedra*, Numer. Math., 121 (2012), pp. 165–204, doi:10.1007/s00211-011-0427-7.

[37] M. Wheeler, G. Xue, and I. Yotov, *Coupling multipoint flux mixed finite element methods with continuous Galerkin methods for poroelasticity*, Comput. Geosci., 18 (2014), pp. 57–75.

[38] M. F. Wheeler and I. Yotov, *A multipoint flux mixed finite element method*, SIAM J. Numer. Anal., 44 (2006), pp. 2082–2106, doi:10.1137/050638473.